Tectonophysics 744 (2018) 93–117

Contents lists available at ScienceDirect

Tectonophysics

journal homepage: www.elsevier.com/locate/tecto

Extensional tectonics during Late Cretaceous evolution of the Southern Central Andes: Evidence from the Chilean main range at ~35°S

Marcia Muñoz[a,b,*], Felipe Tapia[c], Mario Persico[b,d], Mathieu Benoit[e], Reynaldo Charrier[a,d], Marcelo Farías[d], Andrés Rojas[b,d]

[a] Escuela de Ciencias de la Tierra, Facultad de Ingeniería, Universidad Andres Bello, Campus República, Salvador Sanfuentes 2357, Santiago, Chile
[b] Advanced Mining Technology Center (AMTC), Facultad de Ciencias Físicas y Matemáticas, Universidad de Chile, Av. Tupper 2007, Santiago, Chile
[c] Universidad de Buenos Aires, Consejo Nacional de Investigaciones Científicas y Técnicas, Instituto de Estudios Andinos "Don Pablo Groeber" (IDEAN), Facultad de Ciencias Exactas y Naturales, Departamento de Ciencias Geológicas, Int. Güiraldes 2160 (C1428EGA), Buenos Aires, Argentina
[d] Departamento de Geología, Universidad de Chile, Casilla 13518, Correo 21, Santiago, Chile
[e] CNRS-UBO, UMR 6538, IUEM, Place N. Copernic, 29280 Plouzané, France

ARTICLE INFO

Keywords:
Southern Central Andes
Chile
Late Cretaceous-Earliest Paleogene
BRCU
Plan de los Yeuques
Extensional tectonics

ABSTRACT

The study of Late Cretaceous-earliest Paleogene series in the Chilean Andes at ~35°S provides new constraints on the coeval evolution of the area and the Southern Central Andes. These correspond to the continental series of BRCU and the overlying Plan de los Yeuques Formation (PYF). Zircon age determinations reveal that these represent an almost continuous record of deposition, respectively from the Cenomanian-early Campanian to the Campanian-Danian. According to paleogeographic reconstructions, the BRCU series corresponds to the coeval foreland basin deposits, in a near arc position, which was westerly bounded by the earliest Late Cretaceous orogen. Detrital zircon age spectra for this reveal only a Cretaceous component, thus indicating a depocenter disconnected to that represented by coeval synorogenic deposits in Argentina. The volcanic rocks of the PYF record an eastern migration of the magmatic loci into the area at least since ~80 Ma. Its outcrops display a series of syn-sedimentary normal faults indicating extensional conditions throughout its deposition. Its volcanic rocks conform an apparent bimodal suite characterized by arc-like affinities, low pressure conditions for the corresponding magmas, and juvenile isotopic signatures for all the compositional spectra. Comparison and modeling of such compositional characteristics indicate a derivation from parental magmas similar to those currently sourcing the southern segment of the Andean Southern Volcanic Zone (~37–42°S). Altogether these characteristics suggest an extensional intra-arc basin setting for the deposition of this unit probably framed by a normal to thin crust of ~30–35 km. The extensional conditions observed for this unit are also recorded in numerous Late Cretaceous arc deposits along the Andean margin, thus indicating that this corresponds to a regional scale feature. This evidence records a change from Late Cretaceous from compressional to extensional conditions in the arc area which agrees well with major plate tectonic configuration proposed for this time span in the Andean margin.

1. Introduction

The Late Cretaceous-Paleocene evolution of the Southern Central Andes (Fig. 1A) is generally considered to be framed by a continuous compressional regime that started acting in the margin in early Late Cretaceous (e.g. Mpodozis and Ramos, 1989; Vergani et al., 1995; Charrier et al., 2007, 2014). The beginning of this episode is marked by the construction of a cordilleran arc orogenic system and a rear arc domain that passed from a back-arc to a foreland basin stage at ~100 Ma (e.g. Zamora Valcarce et al., 2006; Charrier et al., 1996, 2007, 2014; Tunik et al., 2010; Aguirre-Urreta et al., 2011; Di Giulio et al., 2012, 2016; Armas et al., 2014; Balgord and Carrapa, 2014; Boyce, 2015; Fennell et al., 2015; Balgord, 2016). This has been characterized by studies in the coeval arc (e.g. Charrier et al., 2007, 2014; Boyce, 2015) and rear arc domains (e.g. Charrier et al., 1996, 2014; Zamora Valcarce et al., 2006; Tunik et al., 2010; Aguirre-Urreta et al., 2011; Di Giulio et al., 2012, 2016; Armas et al., 2014; Balgord and Carrapa, 2014; Boyce, 2015; Fennell et al., 2015; Balgord, 2016), yet the ongoing evolution until Paleocene times has been mostly inferred from studies in the latter area. This corresponds to the Neuquén basin domain

* Corresponding author at: Escuela de Ciencias de la Tierra, Facultad de Ingeniería, Universidad Andres Bello, Campus República, Salvador Sanfuentes 2357, Santiago, Chile.
E-mail address: marcia.munoz@unab.cl (M. Muñoz).

https://doi.org/10.1016/j.tecto.2018.06.009
Received 29 December 2017; Received in revised form 19 April 2018; Accepted 13 June 2018
Available online 18 June 2018

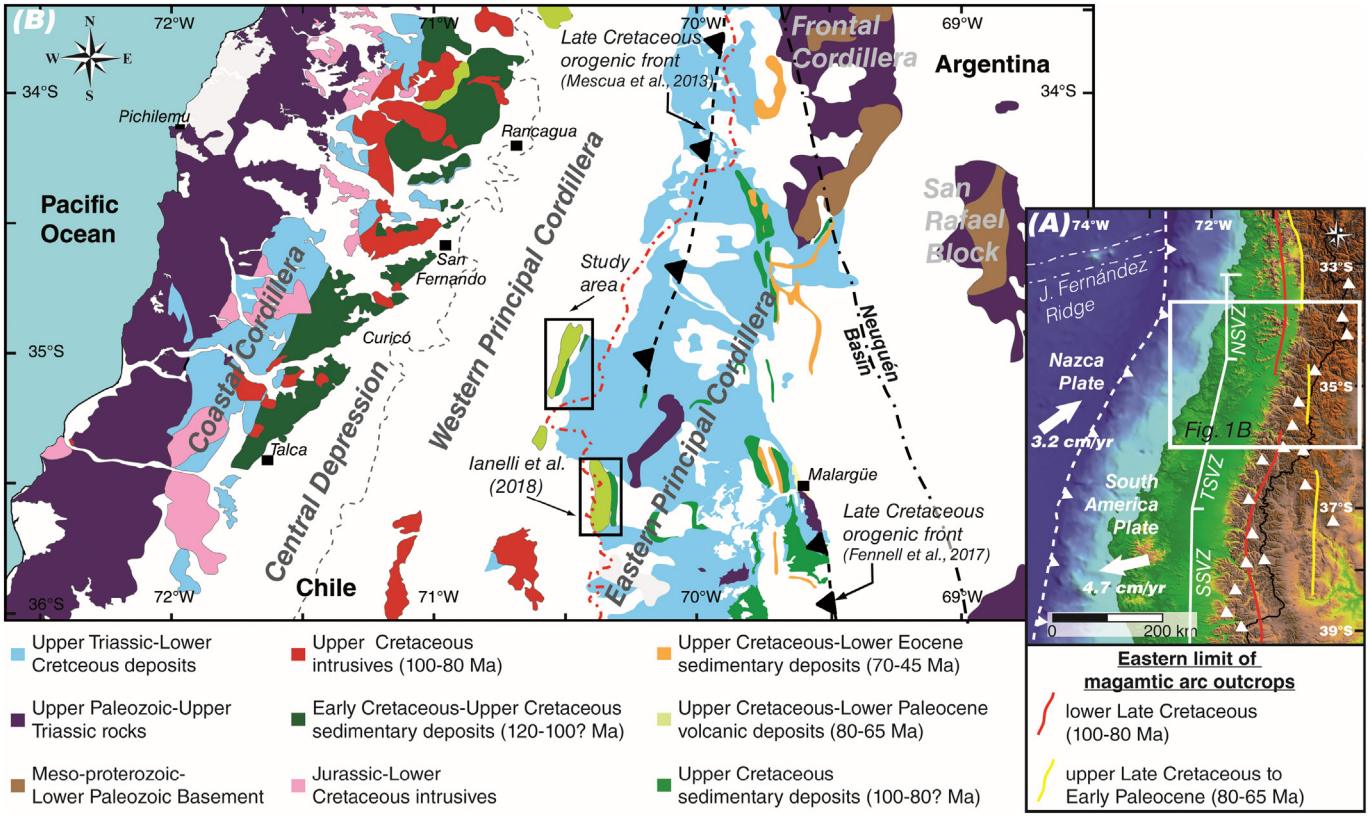

Fig. 1. Main geologic and tectonic features of the margin where the study area is located. (A) Digital Elevation Model (DEM) showing the tectonic setting of the Southern Central Andes. The arrows indicate the absolute plate motion of the Nazca and South America plates. White triangles correspond to main volcanoes of the Southern Volcanic Zone (SVZ). Northern (NSVZ), Transitional (TSVZ) and Southern (SSVZ) segments of the SVZ are shown. Eastern limits of Cretaceous-Paleogene magmatic arc outcrops were defined after Fennell et al. (2015). (B) Simplified geologic map of the Chilean-Argentinean Andean margin between 33° and 37°S showing the morphostructures and lithological units from Mesoproterozoic to Paleocene (modified from Farías et al., 2010; Charrier et al., 2014; Cingolani, 2017, Sernageomin, 2002; Segemar, 1997). Black segmented lines correspond to proposed Late Cretaceous orogenic fronts. Eastern border of the Neuquén basin is shown. The black boxes indicate the position of the study area of this work and that of Iannelli et al. (2018).

(Fig. 1B), in the current foreland in Argentina, where ca. 2000 m of deposits record almost continuously the margin evolution throughout this time span (e.g. Zamora Valcarce et al., 2006; Tunik et al., 2010; Aguirre-Urreta et al., 2011; Di Giulio et al., 2012, 2016; Armas et al., 2014; Balgord and Carrapa, 2014; Balgord, 2016).

In the Chilean slope of the Andes, the complementary record of the Neuquén basin domain during Late Cretaceous times remains poorly studied, which is a consequence of the scarce presence of reported outcrops of this age and the lack of detailed studies on them. According to their westerly position, such units should represent the coeval arc and near rear arc domains and thus they are fundamental for a comprehensive determination of the Late Cretaceous evolution of this area of the margin. Until recent years, the only unit of this age reported in the region corresponded to the BRCU (*Brownish Red Clastic Unit*), a clastic continental series correlated to the basal levels of the Neuquén Group in Argentina (Charrier et al., 1996). According to Charrier et al. (1996), such unit represents deposition during initial subsidence of the foreland basin margin, but proximal to the westerly located volcanic arc. Nevertheless, knowledge on the BRCU is still poor in order to explore its paleogeographic implications against reconstructions made on the much better characterized Neuquén Group. Overlying the BRCU, the recent finding of Upper Cretaceous-Paleocene strata in the region complete the Late Cretaceous record. Such strata were previously assigned to younger units, but field relations and radiometric dating confirmed its correspondence to an independent stratigraphic unit (Mosolf, 2013; Tapia, 2015). They were informally grouped in the Guanaco Unit, which corresponds to a minimum of 2200 m of a continental and predominantly volcanic series representing the coeval arc of this period (Persico et al., 2015; Tapia, 2015; Tapia et al., 2015; Persico, 2016). Following the paleogeographic reconstructions based on the Neuquén Group record and the proposed early Late Cretaceous orogenic architecture (Zamora Valcarce et al., 2006; Tunik et al., 2010; Aguirre-Urreta et al., 2011; Di Giulio et al., 2012, 2016; Balgord and Carrapa, 2014; Fennell et al., 2015; Balgord, 2016), the deposition of this arc series would have had to occur in a wedge top position, or further west into the fold and thrust belt area. The preliminary studies performed in the Guanaco Unit revealed several characteristics which call upon a reassessment of such configuration (Mosolf et al., 2011; Mosolf, 2013; Persico et al., 2015; Tapia, 2015; Tapia et al., 2015; Persico, 2016), hence its relevance for a comprehensive determination of the margin evolution throughout Late Cretaceous times. For such purposes, the predominantly volcanic nature of this series constitutes an additional advantage. Abundant arc magmatic activity is an integral part of Andean evolution and thus it is reflected in several of its characteristics. Features as the location of the arc, the style and nature of igneous products, and the compositional characteristics of magmas have revealed to constitute fundamental tools in tracking their framing geodynamic conditions (e.g. Hildreth and Moorbath, 1988; Haschke et al., 2002; Kay and Mpodozis, 2002; Kay et al., 2005; Mamani et al., 2010).

The object of study of this work is the mentioned Late Cretaceous-Paleocene series in the Chilean Andes at ~35°S. We present the results of an integral geological survey that includes geological mapping, focused on structural and stratigraphic features, and geochronologic and igneous geochemical determinations. This data is used to unravel the context framing the deposition of these series and is integrated and

discussed at local and regional scales. Our results complement the record for the arc and near rear arc domains during the Late Cretaceous-Paleocene and place new constraints on the coeval evolution of the Southern Central Andes in the region.

2. Geological background: the Andean orogen and the Southern Central Andes

The Andes of Chile-Argentina constitute the archetypical example of an active continental margin orogenic system. They distribute as a nearly NS trending belt along the South American continental margin and are a first order result of the eastward subduction of the Nazca oceanic plate underneath it (Fig. 1A). Overall the orogen is a doubly vergent uplifted and deformed area involving Paleozoic to Cenozoic volcanic, sedimentary and crystalline rocks. The Southern Central Andes correspond to the segment of the mountain range distributing between ~33 and 46°S, that is immediately south of the so called flat-slab segment (~27–33°S; Fig. 1A). The current tectonic configuration in this area is characterized by a convergence rate of ~7 cm/y with an obliquity of ~20° (Somoza and Ghidella, 2005) and a subduction dip angle of ~27° (Pardo et al., 2002). Current absolute plate motion relative to hot spots frame for the South America and Nazca plates are 4.8 and 3.2 cm/y, respectively (Fig. 1A; Gripp and Gordon, 2002). Between 33 and 37°S, the Andes are segmented into five NS-trending morphostructural units (Fig. 1B), which from west to east correspond to the: Coastal Cordillera, Central Depression, Principal Cordillera, Frontal Cordillera and Andean Foreland in Argentina. For discussion related to the paleogeography and orogenic evolution, the Principal Cordillera has been subdivided in the following into the Western and Eastern principal cordilleras according to particular geological features. The Western Principal Cordillera corresponds to a fault-bounded Late Cretaceous to Miocene series composed of up to ~5000 m thick igneous and minor sedimentary rocks. The Eastern Principal Cordillera corresponds to a series of sedimentary and minor volcanic Mesozoic units that are involved in east vergent thin- and thick-skinned fold and thrust belts near the Chilean-Argentinean border. The currently active volcanic arc runs along the Eastern Principal Cordillera and the easternmost Western Principal Cordillera (Fig. 1A).

Classically, the construction of the modern Andean orogen is considered to have started in early Late Cretaceous, after a major contractional episode that affected regionally the South American margin (e.g. Mpodozis and Ramos, 1989; Charrier et al., 2007). Recent studies have shown that by that time the whole orogenic system was structured from the Coastal Cordillera (c.f. Arancibia, 2004) up to the eastern fold-and-thrust belt (c.f. Fennell et al., 2015). This deformational period was accompanied the passage of the rear arc domain from a back-arc to a foreland basin, the latter which accumulated the synorogenic deposits of the relief being constructed (e.g. Mpodozis and Ramos, 1989; Charrier et al., 2007; Folguera and Ramos, 2011; Fennell et al., 2015). In addition, the coeval early Late Cretaceous magmatic arc (~100–80 Ma) migrated eastwards and its records are represented in numerous outcrops of volcanic and intrusive rocks of this age exposed in the eastern slope of the Coastal Cordillera and in the Central Depression along the southern Central Andes (Fig. 1A). The following evolution during Late Cretaceous-earliest Paleocene (~80–60 Ma) is less well constrained in the Chilean slope of the Andes, where the arc and near rear arc areas should be recorded, compared to the intensively studied Neuquén basin domain, the coeval foreland basin setting. In the latter region, the sedimentary series that comprise the Neuquén and Malargüe groups have been interpreted to represent the foreland basin stage whose beginning is marked by the contact between the base of the Neuquén Group and the underlying units (Zamora Valcarce et al., 2006; Tunik et al., 2010; Di Giulio et al., 2012, 2016; Balgord and Carrapa, 2014; Fennell et al., 2015). Overall for these groups, provenance studies have shown the variable influence of the westerly located coeval arc, among other sources, which has been attributed to the eastern migration of both the arc itself and the advancing deformation front of the fold and thrust belts that limited the orogen to the east (Zamora Valcarce et al., 2006; Tunik et al., 2010; Aguirre-Urreta et al., 2011; Di Giulio et al., 2012, 2016; Balgord and Carrapa, 2014; Fennell et al., 2015; Balgord, 2016). The eastern migration of the arc during this time is also recorded in the Chilean slope of the Andes, where several local igneous units of this age are placed immediately to the east of the earliest Late Cretaceous arc (Fig. 1A; e.g. Mpodozis and Ramos, 1989; Charrier et al., 2007). However, such process seems to have not been uniform along the margin, as for the region south of 36°S the presence of igneous rocks with arc-like affinities in the Neuquén basin domain accounts for a more drastic migration (Fig. 1A; Llambías and Rapela, 1989; Franchini et al., 2003; Zamora Valcarce et al., 2006; Case et al., 2008; Aguirre-Urreta et al., 2011; Mateo et al., 2011; Spagnuolo et al., 2012; Armas et al., 2014).

3. Analytical methods

Radiometric dating was performed on 10 samples by in-situ U-Pb determinations in single zircon crystals, through the laser ablation method, at the Centro de Geociencias - Universidad Autónoma de México, México (see Supplementary material item 1 and Table 1). Zircon grains were separated from total rock samples using standard crushing, washing, heavy liquid, and paramagnetic procedures at facilities of the Departamento de Geología - Universidad de Chile and of the Carrera de Geología - Universidad Andrés Bello, both in Chile. U–Pb analyses were performed by laser ablation inductively coupled plasma mass spectrometry (LA-ICP-MS) employing a Thermo Xseries QICPMS (FD samples) and a Thermo ICap Qc quadrupole ICPMS (remaining samples), in both cases coupled with a Resolution M050 excimer laser workstation. U and Th concentrations were calculated employing external standard zircons, 91500 (1065.4 ± 0.6 Ma; Wiedenbeck et al., 1995) and Plešovice (337.13 ± 0.37 Ma; Sláma et al., 2008), as in Paton et al. (2010). The isotopic ratios, ages and errors were calculated according to Petrus and Kamber (2012). In the data tables analytical determinations are reported at 2σ uncertainties, which were propagated according to Paton et al. (2010). Analyzed spots were 23 μm, using an analytical protocol modified from Solari et al. (2010), and these were selected after the study of transmitted light and cathodoluminescence images. For each spot a set of trace elements were also measured in order to monitor possible inclusions in zircon crystals, using the NIST-SRM 610 glass as a reference standard and ^{29}Si as an internal standard (15.323% assumed stoichiometric value). The presented concordia plots, probability density plots with stacked histograms, and weighted mean ^{206}Pb/^{238}U age calculations were carried out using ISOPLOT/EX 3.7 (Ludwig, 2008) and DensityPlotter (Vermeesch, 2012). For all age calculations U-Pb data with a

Table 1
Summary of zircon age determinations.

Sample	Age	2σ	Rock type	Unit	Location
MT12	68.6	1.0	Pyroclastic	Plan de los Yeuques Fm.	Tinguiririca valley
MT26	71.1	1.1	Pyroclastic	Plan de los Yeuques Fm.	Tinguiririca valley
ATE22	79.3	2.0	Pyroclastic	Plan de los Yeuques Fm.	Teno valley
ATE27	86.8	1.2	Sedimentary	BRCU	Teno valley
FD12-02	91.3	0.9	Sedimentary	BRCU	Teno valley
FD12-03	92.1	1.4	Sedimentary	BRCU	Tinguiririca valley
FD12-04	93.0	0.8	Sedimentary	BRCU	Tinguiririca valley
FD12-05	95.4	0.3	Sedimentary	BRCU	Tinguiririca valley
FD13-01	75.6	0.5	Pyroclastic	Plan de los Yeuques Fm.	Tinguiririca valley
PT35	69.3	0.5	Dike	Plan de los Yeuques Fm.	Tinguiririca valley
ATE16	19.4	0.7	Pyroclastic	Miocene volcanics	Vergara valley

Table 2
Results of whole rock chemical analyses.

Sample	MT2	MT3	MT6	MT7	MT12	MT13	MT15	MT16	MT19	MT23	PT 35	ATE1	ATE8	ATE26	DL[c]
Rock type	Lava	Lava	Lava	Lava	Pyroclastic	Lava	Lava	Lava	Lava	Lava	Dyke	Lava	Lava	Lava	
Classification[a]	Cpx basalt	Cpx basalt	Px andesite	Px andesite	Vitric ash tuff	Opx andesite	Andesite	Two px andesite	Basaltic andesite	Two px andesite	Hbl tonalite	Px andesite	Px andesite	Hbl dacite	
Comsposition[b]	BA	BA	BA	BA	D	A	BA	A	BA	A	A	A	A	A	
UTM-N	6,134,560	6,133,936	6,134,360	6,133,420	6,133,445	6,133,557	6,133,502	6,134,149	6,132,249	6,131,465	6,131,002	6,118,774	6,119,752	6,116,401	
UTM-E	361,510	362,549	362,171	363,080	362,407	362,651	365,088	363,549	363,564	365,344	368,765	361,393	360,804	361,600	
Major elements in wt%															
SiO_2	49.96	53.78	50.46	50.56	67.02	56.44	52.75	56.05	53.72	56.42	57.52	55.33	57.11	55.71	0.01
Al_2O_3	16.12	19.38	18.75	19.05	14.22	18.04	19.77	16.89	19.19	16.95	17.70	18.10	18.46	19.50	0.01
Fe_2O_3(T)	10.91	8.79	9.89	11.10	3.20	7.61	8.76	9.06	8.72	8.99	6.77	7.88	6.16	5.23	0.01
MnO	0.15	0.17	0.18	0.18	0.10	0.19	0.23	0.15	0.20	0.15	0.16	0.22	0.14	0.24	0.001
MgO	4.85	2.47	4.05	3.67	1.76	1.74	2.66	3.18	2.87	3.07	2.67	2.20	1.70	1.95	0.01
CaO	8.34	8.31	7.48	8.57	4.55	6.16	6.31	6.63	7.53	6.75	6.98	5.65	3.46	6.38	0.01
Na_2O	3.29	3.82	4.26	3.44	1.04	4.58	5.03	3.47	3.84	3.35	3.69	4.28	5.09	4.58	0.01
K_2O	0.63	1.23	1.05	0.55	1.74	2.05	1.78	1.94	1.38	1.97	1.31	2.12	3.99	1.94	0.01
TiO_2	1.00	1.07	1.06	0.98	0.30	0.71	0.76	1.01	0.62	0.96	0.71	0.73	0.36	0.64	0.001
P_2O_5	0.14	0.27	0.24	0.22	0.07	0.41	0.43	0.28	0.39	0.29	0.23	0.26	0.31	0.29	0.01
LOI	3.30	1.07	2.41	1.89	6.24	2.18	1.96	1.70	1.39	1.36	2.39	2.08	2.23	2.45	
Total	98.70	100.40	99.82	100.20	100.20	100.10	100.40	100.40	99.85	100.30	100.10	98.86	99.02	98.90	0.01
Trace elements in ppm															
Sc	23	22	21	19	7	12	14	26	11	25	13	9	5	7	1
Be	bdl	1	1	1	2	2	1	1	1	1	1	1	1	1	1
V	157	145	236	219	36	93	118	218	88	205	123	70	31	61	5
Cr	250	50	40	70	bdl	50	30	70	70	130	30	30	30	70	20
Co	42	15	29	32	4	14	18	21	16	22	12	15	20	18	1
Ni	160	30	40	50	bdl	40	20	40	50	70	bdl	20	20	40	20
Cu	60	90	80	70	bdl	10	20	420	30	130	20	20	20	30	10
Zn	100	60	60	70	100	60	60	90	60	80	70	70	50	60	30
Ga	14	16	14	14	11	13	13	16	12	16	18	16	15	16	1
Ge	1	2	1	2	1	2	1	2	1	2	1	2	1	2	1
As	bdl	bdl	13	bdl	7	bdl	11	16	bdl	11	bdl	8	10	bdl	5
Rb	10	21	17	6	65	44	24	51	24	45	37	35	88	26	2
Sr	539	745	1603	851	814	867	1022	478	884	447	599	889	1026	1148	2
Y	17	23	16	17	25	22	21	26	19	26	21	25	15	21	$2^{(i)}$, $1^{(ii)}$
Zr	69	77	84	65	180	102	88	134	79	131	178	107	105	89	$4^{(i)}$, $2^{(ii)}$
Nb	3	2	3	2	4	3	2	4	2	4	5	3	2	bdl	1
Mo	bdl	bdl	bdl	2	bdl	bdl	bdl	2	2	4	bdl	bdl	2	bdl	2
Ag	bdl	bdl	bdl	bdl	bdl	bdl	bdl	bdl	bdl	bdl	bdl	bdl	bdl	0.9	0.5
In	bdl	bdl	bdl	bdl	bdl	bdl	bdl	bdl	bdl	bdl	bdl	bdl	bdl	bdl	0.2
Sn	bdl	1	bdl	1	2	bdl	bdl	1	bdl	2	bdl	bdl	2	bdl	1
Sb	bdl	bdl	bdl	bdl	bdl	bdl	bdl	bdl	bdl	bdl	bdl	bdl	bdl	1.6	0.5
Cs	0.7	0.5	bdl	bdl	4.1	1.6	1.2	0.6	bdl	0.9	0.7	bdl	1.9	0.6	0.5
Ba	187	357	378	464	382	522	622	489	435	493	526	669	1413	619	$3^{(i)}$, $2^{(ii)}$
La	9.4	12.8	13.5	11.7	23.1	20.0	20.2	19.1	16.9	19.0	22.3	15.2	20.9	17.0	0.1
Ce	20.9	28.9	29.6	25.5	46.6	43.5	43	42.1	37.2	42.2	48.4	35.9	43.1	38	0.1
Pr	2.83	4.02	3.94	3.62	5.36	5.72	5.68	5.56	5.04	5.51	5.93	4.9	5.3	5.03	0.05
Nd	13.4	18.6	17.3	16.3	20.5	25.0	24.4	23.6	22.5	24.0	24.3	21.80	21.80	21.7	0.1
Sm	3.3	4.9	3.9	4.0	4.2	5.5	5.6	5.9	5.0	5.7	4.9	5.5	4.5	5.0	0.1
Eu	1.16	1.59	1.30	1.42	0.75	1.78	1.74	1.42	1.66	1.47	1.51	1.68	1.42	1.69	0.05
Gd	3.4	4.6	3.7	3.8	3.7	4.7	4.7	5.4	4.4	5.3	4.2	4.8	3.5	4.6	0.1
Tb	0.6	0.7	0.5	0.6	0.6	0.7	0.7	0.8	0.7	0.8	0.6	0.8	0.5	0.7	0.1
Dy	3.3	4.1	3.2	3.5	3.7	3.9	3.8	5.1	3.7	4.9	3.6	4.7	3.1	4.2	0.1
Ho	0.7	0.8	0.6	0.7	0.7	0.8	0.8	1	0.7	0.9	0.7	0.90	0.60	0.8	0.1
Er	2	2.4	1.8	2.1	2.4	2.2	2.3	2.9	2	2.8	2.1	2.7	1.8	2.3	0.1
Tm	0.26	0.35	0.25	0.30	0.36	0.33	0.33	0.43	0.30	0.42	0.33	0.4	0.28	0.33	0.05

(*continued on next page*)

Table 2 (*continued*)

Sample	MT2	MT3	MT6	MT7	MT12	MT13	MT15	MT16	MT19	MT23	PT 35	ATE1	ATE8	ATE26	DL[c]
Yb	1.7	2.3	1.6	1.9	2.6	2.2	2.1	2.8	2.0	2.8	2.2	2.7	1.9	2.2	0.1
Lu	0.26	0.39	0.26	0.31	0.46	0.36	0.34	0.44	0.32	0.45	0.34	0.44	0.31	0.39	0.04[(i)], 0.01[(ii)]
Hf	1.8	2.1	2.1	1.8	4.6	2.6	2.4	3.6	2.0	3.5	3.6	2.6	2.4	2.6	0.2
Ta	0.2	0.1	0.1	< 0.1	0.3	0.2	0.1	0.3	0.1	0.3	0.4	0.2	0.1	bdl	0.1
W	bdl	bdl	bdl	bdl	bdl	bdl	bdl	bdl	bdl	bdl	bdl	35	37	42	1
Tl	bdl	bdl	bdl	bdl	bdl	bdl	bdl	bdl	bdl	bdl	bdl	0.1	0.1	bdl	0.1
Pb	bdl	6	bdl	bdl	16	7	7	11	7	10	5	10	14	bdl	5
Bi	bdl	bdl	bdl	bdl	bdl	bdl	bdl	bdl	bdl	bdl	bdl	bdl	bdl	bdl	0.4
Th	1.5	1.6	2.4	1.5	9.6	3	2.4	5.2	1.7	5.1	4.9	2.1	2.7	2.5	0.1
U	0.3	0.4	0.6	0.3	2.1	0.7	0.6	1.4	0.4	1.4	1.1	0.6	0.7	0.7	0.1

Notes: Acronyms DL: detection limits; bdl: below detection limits.

[a] Mineral abbreviations, Cpx: clinopyroxene; Opx: orthopyroxene; Px: pyroxene; Hbl: hornblende.

[b] B: basalt; AB: basaltic andesite; A: andesite; D: dacite.

[c] Detection limits for all samples except otherwise indicated: (i) MT and PT samples, (ii) ATE samples.

discordance over 15% were rejected. For detrital zircon samples maximum depositional age was determined through the weighted mean age of the youngest cluster of three or more grain overlapping at 2σ level following Dickinson and Gehrels (2009). In all samples but one (FD12-04), the ages estimated with this criteria agree with the age of the youngest single zircon, which agrees with the most used and accepted criteria for determining maximum depositional ages (e.g. Dickinson and Gehrels, 2009). For igneous zircon samples the ages were calculated as weighted averages for the statistically coherent populations (Ludwig, 2008).

After U–Pb analyses, Hf isotopes were determined for 3 samples on selected zircon grains employing a Thermo Neptune Plus multi-collector ICP-MS coupled with the mentioned laser workstation. An analytical spot of 44 μm was used, locating it in homogeneous CL zones, right on top of the previous U–Pb analytical spot to ensure that the same dated domain was assessed and thus correctly recalculating the $^{176}Hf/^{177}Hf$ ratios relative to the zircon crystallization age. The external reproducibility of standard zircon grains broadly varied by ± 1 epsilon unit. Each ablation was run for 40 s, with repetitions at 5 Hz rate and an energy density of 6 J/cm^2. The isobaric interferences of ^{176}Lu and ^{176}Yb on the ^{176}Hf signal were corrected by monitoring ^{175}Lu, ^{172}Yb and ^{173}Yb and applying independent mass bias corrections as described in Solari et al. (2017).

For chemical and isotopic whole rock analyses, samples were crushed in a reciprocating steel crusher and subsequently reduced to powder in an agate shatterbox. Whole rock powders were used for analyzing major and trace elements (14 samples; Table 2) and Sr-Nd isotope composition (6 samples; Table 3). Major and trace element analyses were performed at Activation Laboratories, Ontario - Canada, by the procedure 4Litho (www.actlabs.com), which respectively combines ICP-OES and ICP-MS techniques for geochemical determinations. Samples were fused by lithium metaborate/tetraborate and lately diluted for analyses in a Perkin Elmer Sciex ELAN 6000, 6100 or 9000 ICP/MS. Three blanks and five controls (three before sample group and two after) were analyzed per group of samples, duplicates were fused and analyzed every 15 samples, and the instrument was recalibrated every 40 samples. Data quality was controlled by running several standards, relative standard deviations are generally ≤5%, and the detection limits are indicated in Table 2.

Sr-Nd isotopic composition was determined in 6 samples (Table 3) at the CGEO (samples MT2 and MT7) and at the Géosciences Environnement Toulouse laboratory (GET-OMP), France (remaining samples). The analyses at the CGEO were performed using a Thermo Neptune Plus multi-collector ICP-MS following previously established chemical procedures (Gómez-Tuena et al., 2011, 2003). The interference-corrected $^{87}Sr/^{86}Sr$ ratios were exponentially normalized for mass bias to $^{86}Sr/^{88}Sr = 0.1194$ and corrected to a NBS-987 standard ratio of $^{87}Sr/^{86}Sr = 0.710230$. The calculated $^{143}Nd/^{144}Nd$ ratios were exponentially normalized for mass bias to $^{146}Nd/^{144}Nd = 0.72190$, and further corrected to a JNd(i) standard value of $^{143}Nd/^{144}Nd = 0.512115$ (Tanaka et al., 2000), repeatedly measured during the same analytical session. The analyses at the GET-OMP were performed using a TRITON+ Thermo-scientific mass spectrometer. Sr and Nd isotopic compositions were determined after whole rock dissolution. 100 mg of whole rock powder was weighed in a teflon beaker and dissolved in a mixture HF/HNO_3 1:1. After dissolution, samples were dried and then dissolved in 5 ml 2% HNO_3. Aliquots of these solutions were taken, diluted and directly processed through SB-ICPMS in order to get precise [Rb]/[Sr] and [Sm]/[Nd] ratios. The remaining solutions were dried and Nd/Sr was extracted from the matrix using a combination of Sr-Spec, Thru-spec and Ln-Spec resins. An equivalent of 250 ng Sr and 100 ng Nd were run for analyses. NBS987 and La Jolla isotopic standards were regularly run during the measurements. Standard reproducibility was 0.510848 ± 6 (n = 50) for La Jolla and 0.710255 ± 20 (n = 70) for NBS987. Typical blanks are 20 pg for Nd and 150 pg for Sr. The interference-corrected $^{87}Sr/^{86}Sr$ and

Table 3
Results of whole rock Sr-Nd isotopic analyses.

Sample	MT2	MT6	MT7	MT16	MT23	ATE26
Rock type	Lava	Lava	Lava	Lava	Lava	Lava
Classification[a]	Cpx basalt	Px andesite	Px andesite	Two px andesite	Two px andesite	Hbl dacite
Estimated age (Ma)	62	62	73	73	75	80
SiO_2 wt%[b]	53.0	52.3	52.0	57.3	57.6	58.1
Rb	10.0	35.4	6.0	57.1	40.0	25.1
Sr	539.0	1987.0	851.0	517.1	457.7	1153.3
Sm	3.3	3.8	4.0	5.8	5.6	5.2
Nd	13.4	16.7	16.3	25.1	24.1	23.1
$^{87}Sr/^{86}Sr$	0.70391	0.70406	0.70400	0.70422	0.70419	0.70406
2σ	0.000010	0.000005	0.000008	0.000005	0.000004	0.000005
$^{87}Sr/^{86}Sr(i)$	0.70383	0.70401	0.70398	0.70391	0.70393	0.70399
$^{143}Nd/^{144}Nd$	0.512793	0.512800	0.512822	0.512782	0.512783	0.512780
2σ	0.000007	0.000003	0.000008	0.000003	0.000002	0.000003
$^{143}Nd/^{144}Nd(i)$	0.512730	0.512745	0.512750	0.512717	0.512715	0.512709
ε_{Nd}	3.0	3.2	3.6	2.8	2.8	2.8
$\varepsilon_{Nd}(i)$	3.4	3.6	4.0	3.3	3.4	3.4

Notes: In samples MT6, MT16, MT23 and ATE26 the values indicated for Rb, Sr, Sm and Nd have been measured in the same solutions used for isotopic measurements, see Analytical methods for further details.
Isotopic ratios calculations made with decay constants of 6.54×10^{-12} for ^{147}Sm and 1.42×10^{-11} for ^{87}Rb. For $\varepsilon_{Nd}(i)$ values the chondritic ratios of $^{143}Nd/^{143}Nd = 0.512638$ and $^{147}Sm/^{144}Nd = 0.1968$ (Jacobsen and Wasserburg, 1980) were used along with the corresponding estimated formation ages.
[a] Mineral abbreviations, Cpx: clinopyroxene; Px: pyroxene; Hbl: hornblende.
[b] Values in anhydrous basis.

$^{143}Nd/^{144}Nd$ ratios were exponentially normalized for mass bias to $^{88}Sr/^{86}Sr = 8.3752$ and $^{146}Nd/^{144}Nd = 0.7219$.

4. The Southern Central Andes in Chile at ~35°S: geology of the study area

The study area is located in the Western and Eastern Principal cordilleras in Chile, around ~35°S and 70°30′W, in the upper Tinguiririca and Teno river valleys and nearby regions (Figs. 1, 2). The oldest strata distribute along the easternmost part of this area and correspond to Mesozoic sedimentary and subordinately volcanic series deposited in the Neuquén Basin domain (Fig. 2). The upper part of the Mesozoic sequence is represented by the BRCU series and the overlying Upper Cretaceous-Paleocene strata, both of which are the subject of this study and are addressed in detail in the following sections. The area immediately to the west is dominated by outcrops of the Eocene-early Miocene Abanico Formation and also Miocene volcanic and volcanoclastic deposits (Fig. 2). All these Mesozoic and Cenozoic stratigraphic units are variably deformed (e.g. Charrier et al., 2007). The geology is completed by several mostly Miocene to recent intrusive units that crop out dispersedly in the region, and the modern volcanic arc deposits which dominate the highest summits of the range (Fig. 2).

From a regional point of view, main structural features of the study area are related to the Neogene orogenic building of the Andes (e.g. Charrier et al., 2007, 2014; Ramos et al., 1996), but there is also evidence of previous deformational episodes in particular during the Late Cretaceous to Paleocene (e.g. Charrier et al., 1996, 2014; Mescua et al., 2013). The region is characterized by a west dipping homocline fold with N-NE strike involving Mesozoic and Cenozoic rocks (Fig. 3A, B, C). The fold is cut by two NNE-SSW structures: (i) El Fierro and (ii) El Baule thrust faults (Figs. 2, 3D, E). The former is a regional scale east-verging thrust that overrides Paleogene rocks over Mesozoic sequences along the Western Principal Cordillera (Fig. 3A; e.g. Charrier et al., 2014). The El Baule thrust fault overrides Late Cretaceous series over Miocene ones both in the Tinguiririca (Figs. 2, 3B) and Teno valleys (Figs. 2, 3E). Both structures evidence the contractional deformation during Neogene times.

Evidence of pre-Neogene deformation is displayed in the northern slope of the Tinguiririca valley, where the Late Cretaceous deposits are involved in anticline and syncline folds cut by an Eocene dyke constraining the folding (Fig. 3D, E; Mosolf, 2013). Likewise, along the Garcés stream (Fig. 2) the Paleogene Abanico Formation unconformably overlies Late Cretaceous rocks (Fig. 3D, E). In addition to this, along the Vergara river valley, a tributary of the Teno river, Mesozoic rocks are involved in a ENE-WSW trending anticline-syncline system. These correspond to the southernmost structures related to Río del Cobre fault zone (Mescua et al., 2014) which was active during the Late Cretaceous and Miocene (Mescua et al., 2013). This evidence records at least two pre-Eocene contractional periods in the study area, which corresponds to a new finding for the western slope of the Principal Cordillera where only Cenozoic deformation had been recognized.

5. Late Cretaceous series in the Chilean Andes at ~35°S

5.1. BRCU (Cenomanian-early Campanian)

The BRCU corresponds to a clastic continental series, of marked brownish red coloration, originally reported by Charrier et al. (1996) from studies in the upper Tinguiririca valley (Fig. 2). In this area, the BRCU presents a wedge shape with a westward growth reaching a maximum thickness of ~230 m (Fig. 3A). It is composed of a sedimentary basal breccia followed by a series of conglomerates and conglomeratic sandstones with intercalations of finer levels of mudstones and sandstones (Fig. 4A; Charrier et al., 1996). Clasts composition indicate provenance from a predominantly volcanic source (Charrier et al., 1996). Also in the Tinguiririca area, the BRCU overlays in apparent conformity the Baños del Flaco Formation (Late Jurassic-Early Cretaceous; Charrier et al., 1996) and is overlain discordantly by the Abanico Formation (Fig. 3A). Charrier et al. (1996) assigned an age of Late Cretaceous to this unit, based on the stratigraphic position and fossil content, and thus correlated it to the Neuquén Group present in Argentina. According to these authors, the gradual upward fining and thinning shown by the BRCU indicates retrograding deposition during the initial subsidence of a basin margin. This and the correlation with the Neuquén Group in Argentina has led to the consideration of the BRCU series as deposited during the foreland basin stage of the Neuquén Basin evolution (Charrier et al., 1996, 2014). This domain would have been fed mostly by the orogen being constructed westwards, after the early Late Cretaceous compressive event that affected regionally the margin (Charrier et al., 1996, 2014; Mescua et al., 2013).

In order to better constrain the age of the BRCU at its type locality, we performed three age determinations in detrital zircon crystals in

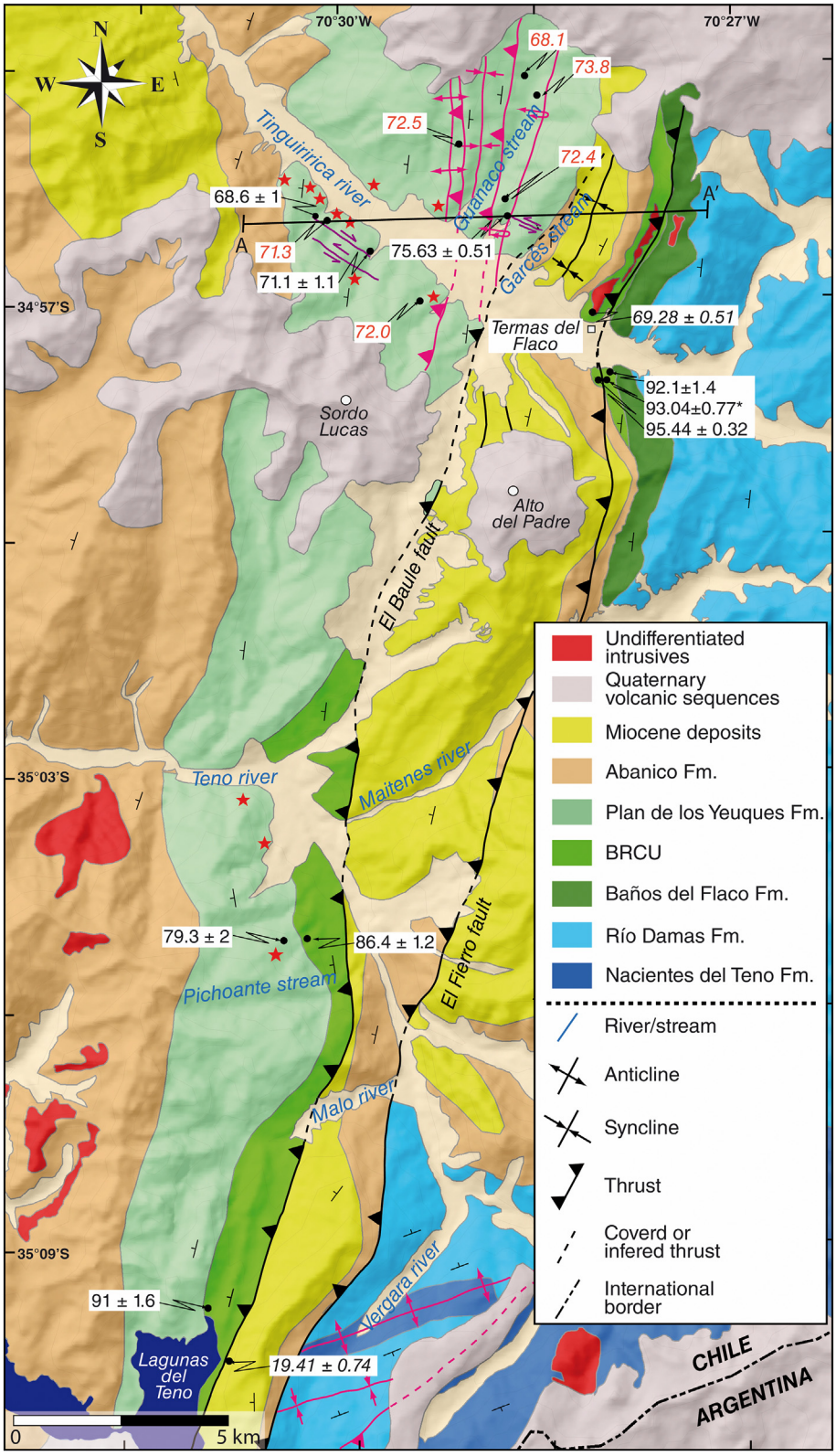

Fig. 2. Geological map of the study area. The numbers in the white rectangles correspond to U-Pb zircon ages obtained in this study (black) and by Mosolf et al. (2011; red). Red stars indicate the location of samples with geochemical analyses. Black cursive ages correspond to samples of Miocene deposits (ATE16) and a Cretaceous dyke (PT35) collected in Laguna del Teno and Tinguiririca river respectively. Geochronological plots of the latter samples are included in the Supplementary material (item 2). Red structures correspond to faults and folds with evidence of pre-Neogene activity. Purple faults show activity during the deposition of the Late Cretaceous Plan de los Yeuques Formation. The trace of the A–A′ cross section presented in Fig. 3E is shown. (For interpretation of the references to color in this figure legend, the reader is referred to the web version of this article.)

samples of this unit from the upper Tinguiririca river valley (Figs. 2 and 3A). For valid data (see Analytical methods and Table 1), zircon age spectra of all samples show mostly Cretaceous ages with major populations around 93–110 Ma (Fig. 5A; Table 1). The maximum depositional ages obtained correspond to 92 ± 1.4, 93 ± 0.8 and 95 ± 0.3 (all ages indicated at 2σ level), respectively for samples FD12-03, FD12-04 and FD12-05 (Fig. 5B; Table 1), and thus this establishes a maximum depositional age for the BRCU of ~95 Ma.

The BRCU has proven to be a difficult unit to identify in the Chilean Andes stratigraphy and thus until the work of Charrier et al. (1996) it was overlooked. This results from its resemblance in the field with the Colimapu Formation, a red continental clastic series of Albian-Aptian age defined further north in the Chilean Andes at ~34°S (upper Maipo river valley; Klohn, 1960). At its type locality, the Colimapu Formation

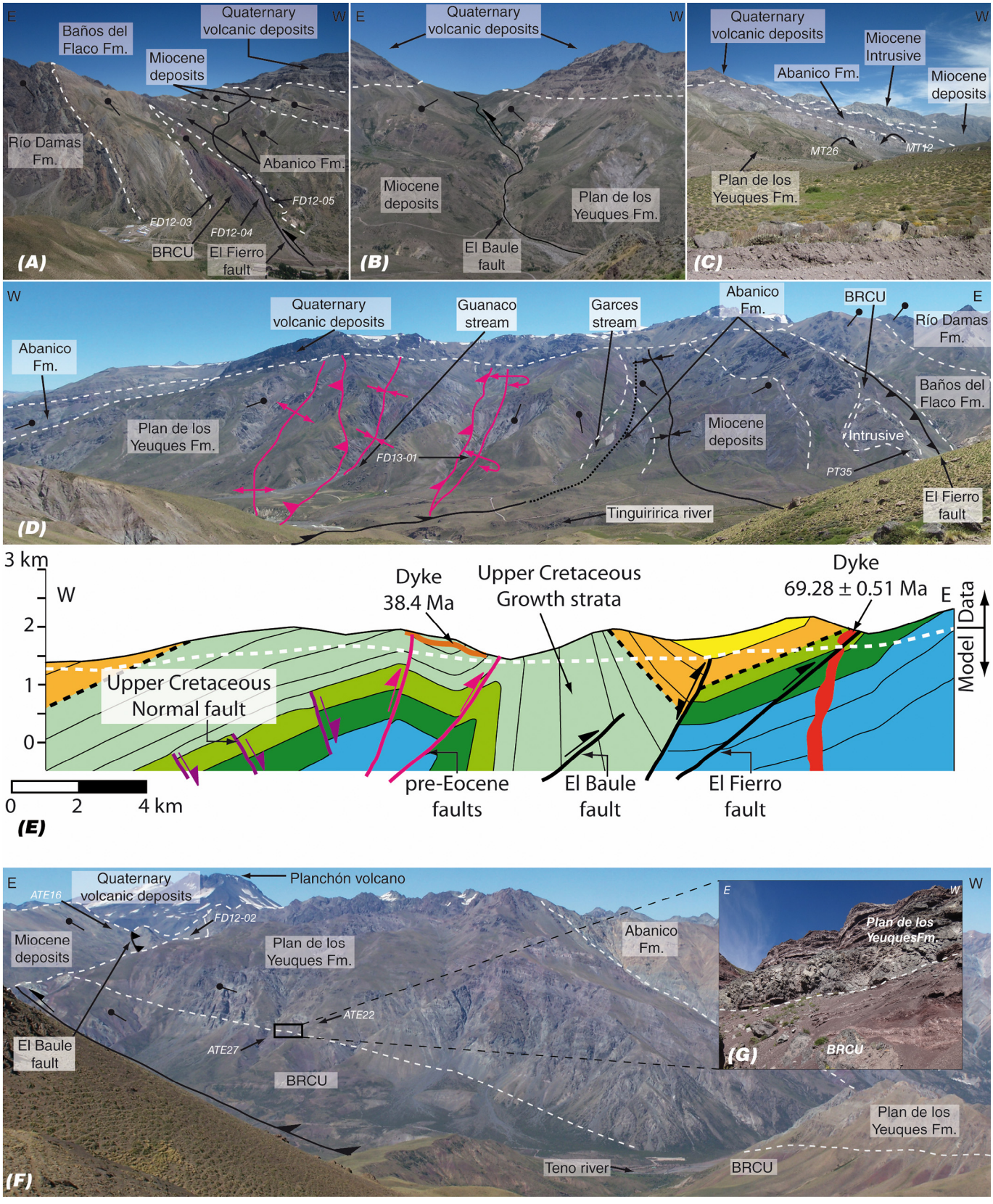

Fig. 3. Main field characteristics of the study area. (A) Southward view of the southern slope of the Tinguiririca river valley showing the contact between Late Jurassic and Early Cretaceous deposits and BRCU. Locations of BRCU samples are shown. (B) Outcrops of the El Baule fault which overrides to the east the Plan de los Yeuques Formation on Miocene deposits. (C) View to the southwest of the Tinguiririca river valley indicating the locations of the dated samples of the Plan de los Yeuques Formation. (D) Northward view of the northern side of the Tinguiririca river valley. Magenta faults and folds correspond to structure with evidence of pre-Neogene activity. (E) Schematic cross-section A–A′ showing the main structural features of the study area (see Fig. 2 for location). (F) Southward view of the Teno river valley. (G) Pseudo-concordant contact between Plan de los Yeuques Formation and BRCU. (For interpretation of the references to color in this figure legend, the reader is referred to the web version of this article.)

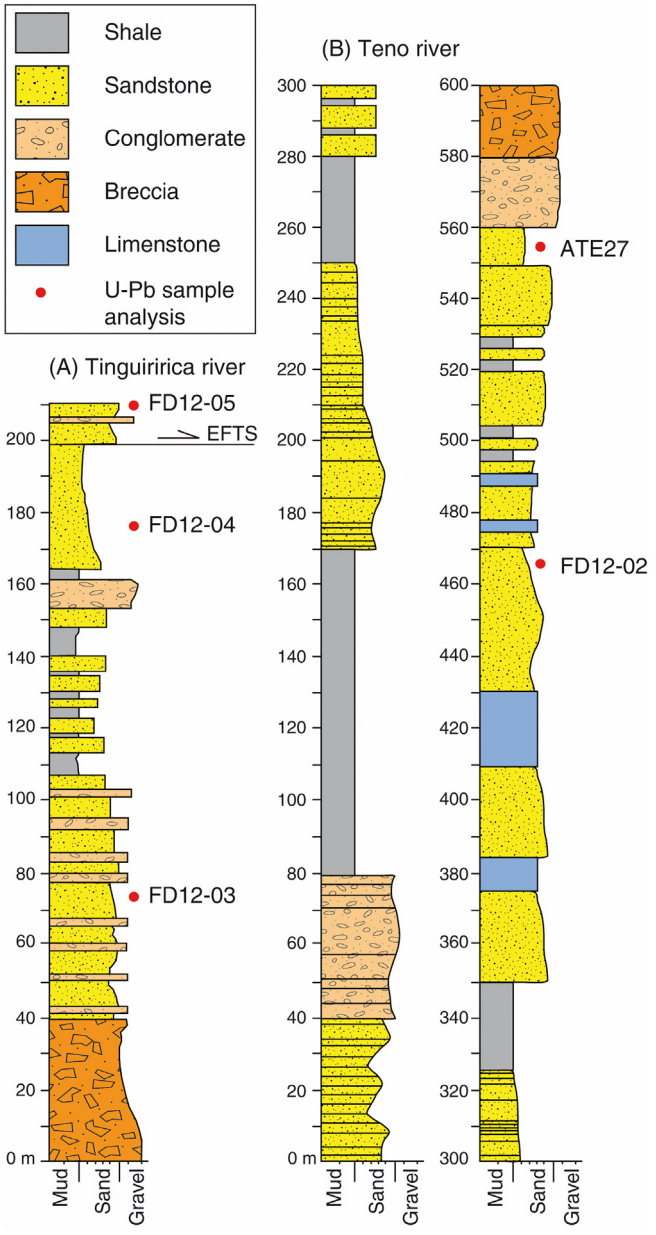

Fig. 4. Stratigraphic section of the BRCU at the Tinguiririca (A) and the Teno (B) valley areas. Section of the BRCU in the latter location is based on González and Vergara (1962).

corresponds to mostly fine grained deposits with thin calcareous intercalations which represent the last regressive episode in the region at the end of the Early Cretaceous (Klohn, 1960). Both based in its fossiliferous content and stratigraphic position, an Albian-Aptian age was assigned to this unit (Klohn, 1960; Martínez-Pardo and Osorio, 1963). Further south from the study area, in the main Andes at ~36°S, one detrital zircon age was reported for the basal section of strata assigned to the Colimapu Formation (Maule river; Astaburuaga, 2014). The obtained ages range from 120 to 140 Ma and thus bracket the lower age limit of this unit to the Barremian-Aptian. These findings confirm the presence of the Colimapu Formation at regional scale in the Chilean Andes stratigraphy, yet this corresponds to a different and significantly older unit than the red continental clastic deposits grouped in the BRCU series.

An assignation to the Colimapu Formation was given by González and Vergara (1962) to a ~600 m thick series of similar characteristics in the southern part of the study area, along the Teno and Vergara river valleys and nearby localities (Figs. 2, 4). Later, Piquer et al. (2010) assigned this same unit to the Abanico Formation (Eocene-early Miocene; Charrier et al., 2002). We obtained two detrital zircon ages for samples collected from the middle (FD12-02) and the upper (ATE27) portion of this series, the latter below its contact with the overlying Plan de Los Yeuques Formation (Figs. 2, 3F; González and Vergara, 1962). Sample FD12-02 shows an age spectrum similar to those obtained in the Tinguiririca area with mostly Cretaceous ages and major populations around 93–110 Ma (Fig. 5A; Table 1). In turn, the age spectrum of sample ATE27 shows Cretaceous ages with major populations between 84 and 97 Ma (Fig. 5A; Table 1). The results show maximum depositional ages of 91 ± 0.9 (FD12-02) and 86 ± 1.2 Ma (ATE27; Fig. 5B) which assign this series to the Late Cretaceous and evidence its stratigraphic correspondence to the BRCU cropping out immediately to the north (Fig. 2).

Considering the maximum age determined for the BRCU along with the oldest one for the overlying unit (see the following), an age range between ~95 and 80 Ma can be inferred for its deposition. In a whole, a Cenomanian-early Campanian age can be assigned to this series thus confirming that this corresponds to a different stratigraphic unit than the Albian-Aptian Colimapu Formation. Given these results, previous assignments of the BRCU to the latter formation in the study area should be disregarded (e.g. González and Vergara, 1962), the same as their consideration as part of the Abanico Formation (Piquer et al., 2010). The BRCU nomenclature is adopted hereafter in this work to refer to such continental red clastic deposits of Cenomanian-early Campanian age.

5.2. *Guanaco Unit and Plan de los Yeuques Formation (Campanian-Danian)*

The Guanaco Unit corresponds to an informal denomination given by Tapia (2015) to a predominantly volcanic continental series of early Campanian-Danian age that crops out along the upper Tinguiririca river valley (Fig. 2). In this area, such unit reaches a minimum thickness of ~2200 m (Fig. 6A), its base is not exposed, and it underlies the Abanico Formation with an angular discordance (Fig. 3D). It consists of lava flows, tuffs and volcanic breccias, with minor sedimentary intercalations, defining an apparent bimodal suite between the effusive and the explosive facies (Fig. 6A). This unit was previously assigned to the lower portions of the Abanico Formation (e.g. Charrier et al., 1996; Zapatta, 1995; Mosolf et al., 2011), due to its similar volcanic nature (Fig. 3D), yet radiometric dating indicates that this corresponds to a different stratigraphic unit.

The first recognition of Upper Cretaceous strata in the region was made by Mosolf et al. (2011) who reported several ages between 63 and 74 Ma in the Tinguiririca area (Ar-Ar and U-Pb radiometric determinations). Our radiometric determinations in this series support such results, with obtained ages of 76 ± 1, 71 ± 1 and 69 ± 1 for three tuffs of the series (samples FD13-01, MT12, MT26; Figs. 2, 3C, 7), in addition to 69 ± 1 Ma for a dioritic dyke (sample PT35; Figs. 2, 3D and Supplementary material item 2). This data reveals the existence of a stratigraphic hiatus in the area of a maximum of ~16 m.y. between the oldest age obtained for the Abanico Formation (~47 Ma; Mosolf et al., 2011) and the youngest age obtained for the Guanaco Unit (~63 Ma; Mosolf et al., 2011). Such hiatus is of regional character in the Chilean geology, being documented elsewhere in the nature of the contact between Mesozoic and Cenozoic units (e.g. Gana and Wall, 1997; Charrier et al., 2007 and references therein). Moreover, in the northern slope of the Tinguiririca valley, the Guanaco Unit strata is folded in an anticline-syncline system cut by 38.4 Ma old dykes (Fig. 3D, E; Mosolf, 2013), thus recording a contractive deformation episode before such age. This evidence supports the consideration of the Guanaco Unit as a single stratigraphic series which represents a previous and different stage respect to the Paleogene extension represented by the Abanico basin deposits.

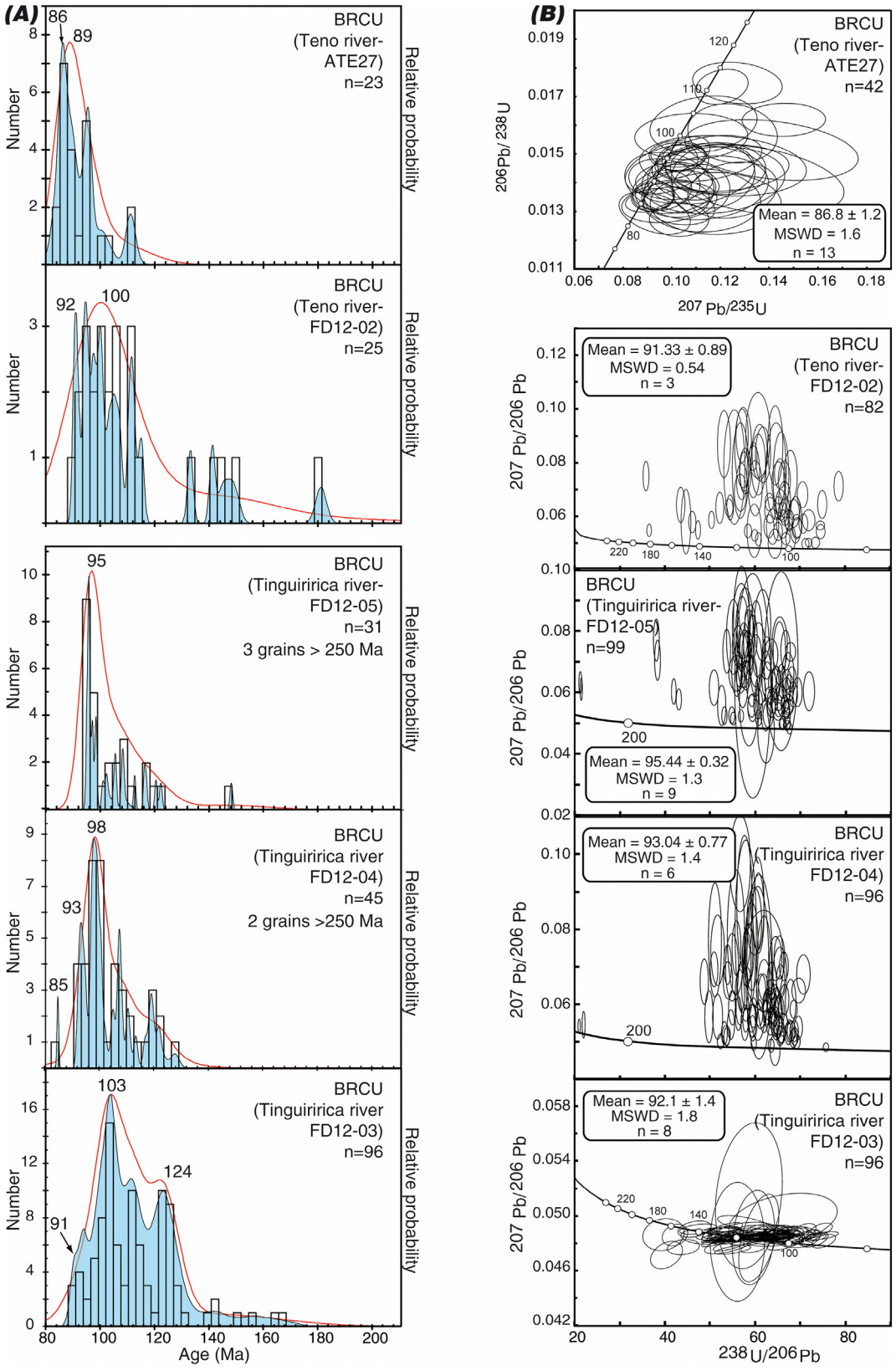

Fig. 5. U-Pb age determinations in detrital zircons of the BRCU. (A) Frequency histograms, relative probability density plots (blue solid area) and kernel density estimators (red line), and (B) Tera-Wasserburg plots. Error ellipses are indicated at 2σ level. (For interpretation of the references to color in this figure legend, the reader is referred to the web version of this article.)

Fig. 6. Stratigraphic section of the Plan de los Yeuques Formation in Tinguiririca (A) and Teno (B) river valleys. Section of the Teno area is based on González and Vergara (1962) and Piquer et al. (2010).

The outcrops of the Guanaco Unit can be continuously followed southwards in the field into the Teno river valley, the southern part of the study area (Fig. 2). In this locality, they were grouped by González and Vergara (1962) in the Plan de los Yeuques Formation, which the authors recognized discontinuously present along the main Chilean Andes at least until 37°15′S. In the Teno valley, the base of this unit is clearly exposed as a pseudo-concordant marked contact passing from the fine stratified red beds of the BRCU series to the coarse stratified massive tuffs and lavas of the Plan de los Yeuques Formation (Fig. 3F, G). In the strata above the contact, we performed a zircon age determination in a tuff which yielded a weighted average age of 79 ± 2 Ma (sample ATE22; Figs. 2, 3F, 7B; Table 1). Altogether, the radiometric age determinations assign the volcanism represented by the Guanaco Unit and the Plan de los Yeuques Formation to an age range between early Campanian-Danian. Given their direct correspondence, the Guanaco Unit strata should be considered as part of the Plan de los Yeuques Formation, a unit formally defined in the Chilean stratigraphy and present at regional scale along the main range (González and Vergara, 1962). This nomenclature is adopted in this work hereafter. It must also be stressed that, for the Teno valley area, previous assignments of the Plan de Los Yeuques Formation strata to the Abanico Formation should be disregarded (e.g. Piquer et al., 2010).

A distinctive characteristic of the Plan de los Yeuques Formation is a series of NNW-SSW synsedimentary normal faults, from centimetric to hectometric scales, which cut the unit and accommodate space for its deposition (Figs. 2, 8). In the southern slope of the Tinguiririca valley, a fault with a normal displacement of at least 300 m accommodates a series of red lavas and tuffs of this unit (Fig. 8A). The thickness of the series above the footwall almost doubles that above the hanging wall, thus evidencing that this corresponds to a syndepositional structure. Similarly, in the Garcés stream area, several normal faults with a vertical slip from 2 to 90 m accommodate the deposition of overturned red tuff strata of the series (Fig. 8B, C). A progressive unconformity in the front-limb of the overturned east-vergent anticline to the east of the Guanaco stream area (Figs. 2, 8D) indicates a growth of the unit although it is not possible to identify the growth direction. Altogether, these observations along with the ~2200 m thickness of the series indicate extensional conditions during its deposition, at least during the accumulation of the lower levels where the normal faults were recognized.

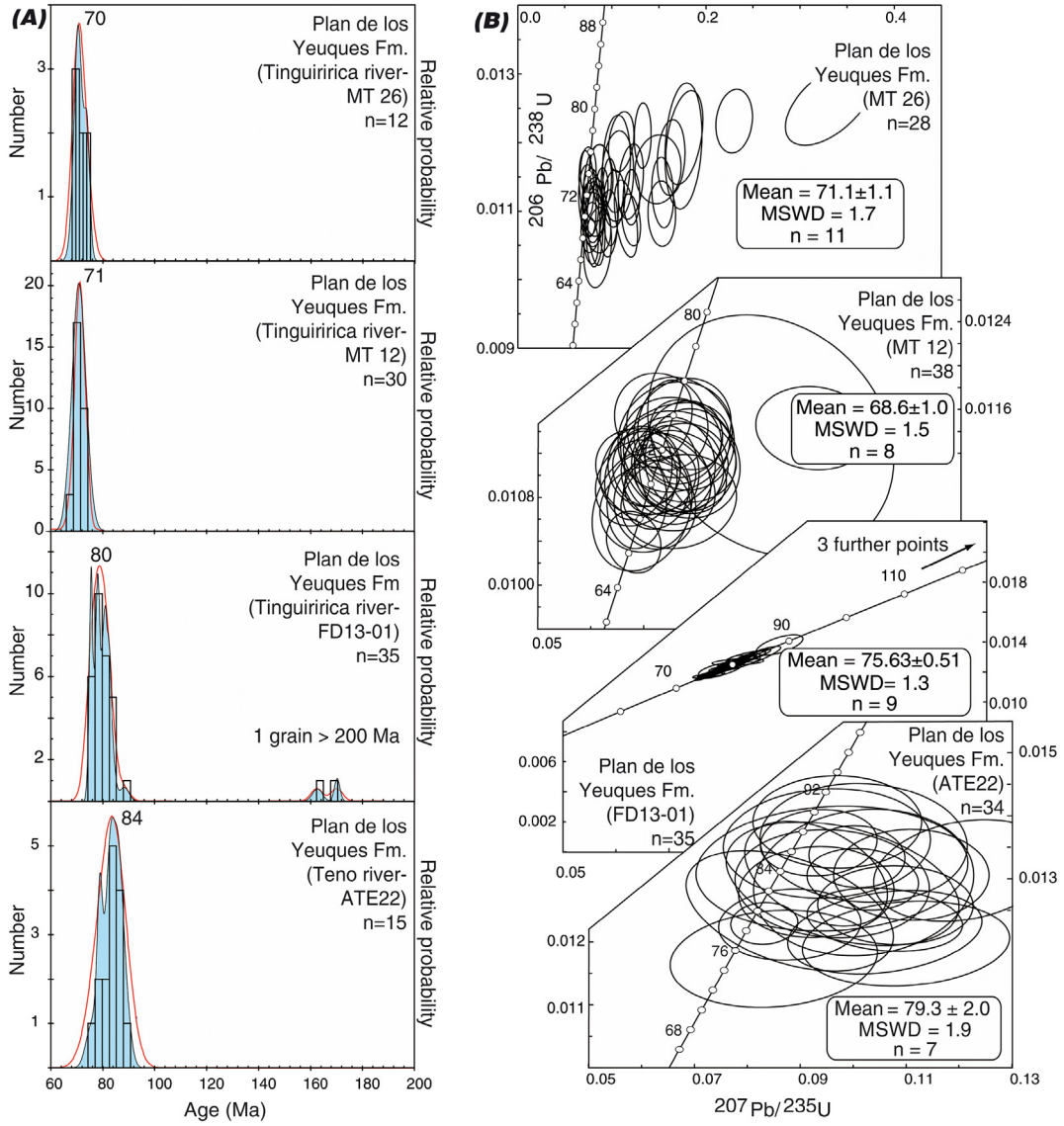

Fig. 7. U-Pb age determinations in igneous zircons of the Plan de los Yeuques Formation. (A) Frequency histograms, relative probability density plots (blue solid area) and kernel density estimators (red line), and (B) Tera-Wasserburg plots. Weighted mean ages are shown in Tera-Wasserburg plots. Error ellipses are indicated at 2σ level. (For interpretation of the references to color in this figure legend, the reader is referred to the web version of this article.)

6. Geochemistry of Upper Cretaceous igneous units

Geochemical determinations were performed in 14 igneous samples belonging to Plan de los Yeuques Formation in the Tinguiririca (n = 11; n: number of samples) and Teno (n = 3) river valleys (Figs. 2, 6A, B). These include whole rock major and trace element composition (n = 14; Table 2) and Sr-Nd isotopic determinations (n = 6; Table 3). Rock samples correspond to olivine and/or pyroxene basalts, basaltic andesites and andesites, and one vitric tuff, with a primary mineralogy composed of plagioclase, olivine, orthopyroxene, clinopyroxene, iron oxides, and accessory apatite, in addition to scarce amphibole and zircon present only in the acidic tuffs (Persico, 2016). Hf isotopic composition was also determined in 3 dacitic tuffs with zircon age determinations (Table 4). Alteration is a common feature in all rocks from these units and is represented in the variable presence of low-grade minerals as chlorite/smectite, epidote, prehnite, calcite, titanite, iron oxides and clays (Persico, 2016). Analyzed samples were selected after standard optical studies and show a minor degree of alteration which has not affected their primary compositional characteristics (see the following; LOI < 3.3 wt% for all samples except the tuff with 6.2 wt%; Table 2).

Studied samples show a range in SiO_2 contents between 51 and 71% yet this is composed by a group of mostly basic compositions, with SiO_2 contents between 51 and 59%, and the single tuff analyzed, with a SiO_2 content of 71% (all values given in anhydrous basis; Fig. 9A). Altogether, the compositional range defines a gap of ~13% SiO_2 between basic and acid members thus conforming an apparent bimodal suite. The underrepresentation of acid members results from the high degree of alteration and/or the high lithic clast content of pyroclastic rocks which precluded performing reliable analyses. Nevertheless, despite that the mentioned compositional gap could be reduced, such bimodal character is widely recorded in the field in the monotonous intercalations of basic lava flows and acid pyroclastic deposits that dominate the ~2200 m thickness of the studied series (Fig. 6). In terms of chemical affinities (Fig. 9), the rock suite shows a subalkaline character with an arc signature as shown in tectonic discrimination diagrams based on trace element composition (not shown). Calc-alkaline to tholeiitic affinities are variably suggested by different classification schemes

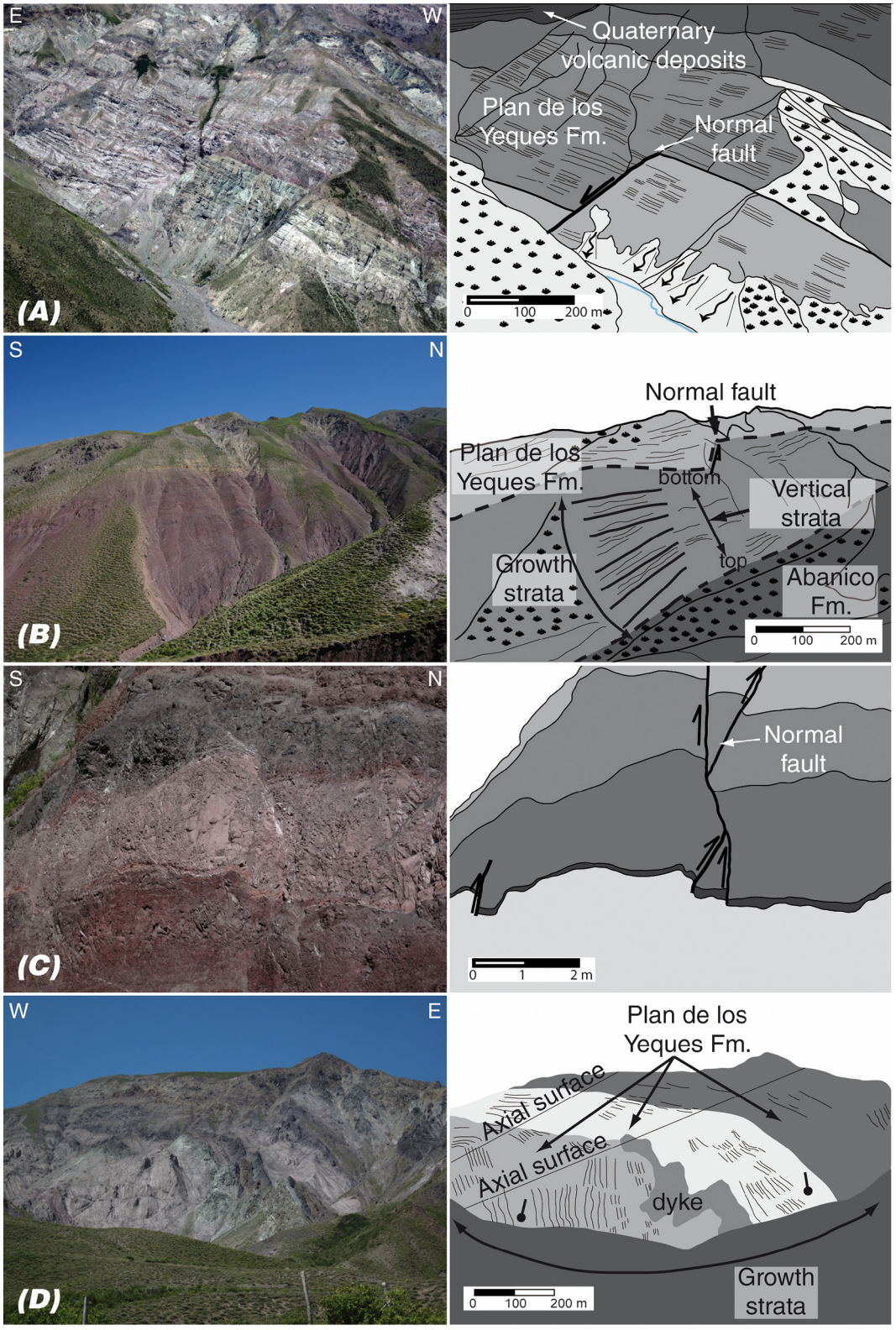

Fig. 8. Normal faulting in the Plan de los Yeuques Formation. (A) Normal fault in the southern slope of the Tinguiririca valley controlling the deposition > 200 m of Late Cretaceous volcanic deposits. (B) Southward growth strata on overturned volcanic deposits in the Garcés stream area. Note the > 200 m thickness showing the growth. (C) In the same area, overturned normal faults as long as 2 m accommodate the deposition of volcanoclastic deposits. (D) Growth strata in the front limb of an anticline fold, to the west of the Garcés stream.

Table 4
Results of zircon Hf isotopic determinations.

#		$^{176}Hf/^{177}Hf$	2σ	$^{176}Lu/^{177}Hf$	$2\sigma^{(2)}$	$^{176}Hf/^{177}Hf(t)$	t (Ma)	ε_{Hf}	2σ	$\varepsilon_{Hf}(t)$	2σ
ATE22		Lithic lapilli tuff; 6,116,446N-361,671E									
1	Zircon_64	0.282949	0.000028	0.002335	0.000055	0.282945	81.9	5.8	1.0	7.5	1.0
2	Zircon_67	0.282984	0.000033	0.002321	0.000038	0.282980	86.8	7.0	1.2	8.8	1.2
3	Zircon_69	0.282983	0.000033	0.003284	0.000048	0.282978	84.2	7.0	1.2	8.7	1.2
4	Zircon_70	0.282943	0.000037	0.000198	0.000007	0.282943	78.8	5.6	1.3	7.3	1.3
5	Zircon_71	0.282983	0.000033	0.002711	0.000016	0.282979	82.9	7.0	1.2	8.7	1.2
6	Zircon_73	0.282962	0.000030	0.002928	0.000010	0.282958	79.1	6.3	1.1	7.9	1.1
7	Zircon_75	0.282980	0.000036	0.002571	0.000052	0.282976	80.6	6.9	1.3	8.5	1.3
8	Zircon_77	0.282983	0.000035	0.002742	0.000067	0.282979	83.8	7.0	1.2	8.7	1.2
9	Zircon_80	0.282976	0.000088	0.002247	0.000011	0.282973	76.7	6.8	3.1	8.3	3.1
10	Zircon_81	0.283030	0.000040	0.003011	0.000010	0.283025	86.9	8.7	1.4	10.4	1.4
11	Zircon_82	0.282948	0.000036	0.002811	0.000044	0.282944	77.9	5.8	1.3	7.4	1.3
12	Zircon_83	0.282983	0.000037	0.002986	0.000056	0.282979	78.6	7.0	1.3	8.6	1.3
13	Zircon_84	0.282991	0.000035	0.002775	0.000043	0.282987	82.8	7.3	1.2	9.0	1.2
14	Zircon_85	0.282961	0.000030	0.002830	0.000029	0.282957	83.6	6.2	1.1	7.9	1.1
15	Zircon_86	0.282940	0.000057	0.002786	0.000018	0.282936	75.2	5.5	2.0	7.0	2.0
16	Zircon_87	0.282977	0.000033	0.003229	0.000025	0.282972	85.5	6.8	1.2	8.5	1.2
17	Zircon_88	0.283016	0.000036	0.002707	0.000027	0.283011	89.0	8.2	1.3	10.0	1.3
18	Zircon_89	0.282925	0.000053	0.002802	0.000037	0.282921	83.2	5.0	1.9	6.6	1.9
19	Zircon_91	0.282933	0.000027	0.002287	0.000019	0.282929	84.1	5.2	1.0	7.0	1.0
20	Zircon_92	0.282961	0.000032	0.002623	0.000025	0.282957	86.9	6.2	1.1	8.0	1.1
21	Zircon_95	0.282963	0.000031	0.002131	0.000017	0.282960	80.0	6.3	1.1	8.0	1.1
MT12		Dacitic vitric tuff; 6,133,445N-362,407E									
1	Zircon_93	0.282956	0.000030	0.001669	0.000024	0.282954	73.2	6.0	1.1	7.6	1.1
2	Zircon_95	0.283018	0.000026	0.000923	0.000013	0.283017	68.5	8.2	0.9	9.7	0.9
3	Zircon_97	0.282981	0.000027	0.001332	0.000081	0.282979	71.5	6.9	1.0	8.5	1.0
4	Zircon_98	0.282992	0.000028	0.001614	0.000009	0.282990	72.7	7.3	1.0	8.9	1.0
5	Zircon_99	0.283026	0.000029	0.001278	0.000012	0.283024	70.3	8.5	1.0	10.0	1.0
6	Zircon_100	0.282973	0.000022	0.001365	0.000074	0.282971	69.0	6.6	0.8	8.1	0.8
7	Zircon_102	0.283014	0.000046	0.004250	0.000280	0.283008	73.0	8.1	1.6	9.5	1.6
8	Zircon_107	0.282988	0.000029	0.001624	0.000015	0.282986	73.7	7.2	1.0	8.7	1.0
9	Zircon_108	0.282974	0.000024	0.001695	0.000032	0.282972	69.5	6.7	0.8	8.1	0.8
10	Zircon_110	0.283001	0.000033	0.002149	0.000022	0.282998	70.3	7.6	1.2	9.1	1.2
11	Zircon_111	0.283003	0.000031	0.001627	0.000043	0.283001	70.2	7.7	1.1	9.2	1.1
12	Zircon_112	0.282985	0.000023	0.001880	0.000009	0.282983	70.8	7.1	0.8	8.6	0.8
13	Zircon_113	0.282967	0.000027	0.001910	0.000014	0.282965	66.6	6.4	1.0	7.8	1.0
14	Zircon_116	0.282996	0.000032	0.001688	0.000028	0.282994	70.9	7.5	1.1	9.0	1.1
15	Zircon_118	0.282951	0.000028	0.001451	0.000005	0.282949	68.8	5.9	1.0	7.3	1.0
16	Zircon_120	0.282978	0.000029	0.001610	0.000010	0.282976	68.6	6.8	1.0	8.3	1.0
17	Zircon_122	0.283022	0.000033	0.001789	0.000011	0.283020	73.6	8.4	1.2	9.9	1.2
18	Zircon_123	0.283008	0.000032	0.001652	0.000021	0.283006	71.0	7.9	1.1	9.4	1.1
19	Zircon_125	0.282990	0.000031	0.001240	0.000016	0.282988	71.0	7.2	1.1	8.8	1.1
MT26		Dacitic vitric tuff; 6,132,558N-363,719E									
1	Zircon_127	0.283017	0.000029	0.001656	0.000070	0.283015	69.0	8.2	1.0	9.7	1.0
2	Zircon_130	0.283009	0.000040	0.001876	0.000036	0.283007	67.8	7.9	1.4	9.3	1.4
3	Zircon_131	0.283008	0.000038	0.001938	0.000013	0.283005	71.3	7.9	1.3	9.4	1.3
4	Zircon_132	0.282993	0.000033	0.001460	0.000020	0.282991	74.9	7.4	1.2	8.9	1.2
5	Zircon_133	0.282979	0.000032	0.001534	0.000016	0.282977	73.9	6.9	1.1	8.4	1.1
6	Zircon_135	0.283006	0.000041	0.002674	0.000059	0.283002	72.8	7.8	1.4	9.3	1.5
7	Zircon_136	0.282994	0.000026	0.001495	0.000041	0.282992	70.9	7.4	0.9	8.9	0.9
8	Zircon_137	0.282977	0.000038	0.001573	0.000014	0.282975	68.9	6.8	1.3	8.2	1.3
9	Zircon_139	0.282992	0.000032	0.001688	0.000037	0.282990	67.2	7.3	1.1	8.7	1.1
10	Zircon_140	0.282983	0.000030	0.001095	0.000007	0.282982	73.1	7.0	1.1	8.6	1.1
11	Zircon_142	0.283022	0.000043	0.001917	0.000034	0.283020	69.5	8.4	1.5	9.8	1.5
12	Zircon_144	0.282923	0.000061	0.002359	0.000065	0.282920	69.4	4.9	2.2	6.3	2.2
13	Zircon_145	0.283005	0.000031	0.001372	0.000010	0.283003	70.6	7.8	1.1	9.3	1.1
14	Zircon_146	0.283035	0.000070	0.001926	0.000026	0.283032	71.0	8.8	2.5	10.3	2.5
15	Zircon_148	0.283024	0.000046	0.002045	0.000011	0.283021	70.1	8.5	1.6	9.9	1.6
16	Zircon_150	0.283008	0.000030	0.001392	0.000007	0.283006	71.6	7.9	1.1	9.4	1.1
17	Zircon_153	0.283002	0.000037	0.002015	0.000036	0.282999	69.4	7.7	1.3	9.1	1.3
18	Zircon_156	0.283022	0.000030	0.001717	0.000040	0.283020	77.0	8.4	1.1	10.0	1.1
19	Zircon_157	0.283036	0.000042	0.001722	0.000010	0.283034	74.2	8.9	1.5	10.4	1.5
20	Zircon_160	0.283024	0.000057	0.001794	0.000015	0.283022	73.1	8.5	2.0	10.0	2.0

Notes: Söderlund et al. (2004) ^{176}Lu decay constant of 1.867×10^{-11} has been used in these calculations. For ε_{Hf} calculation the chondritic values of Blichert-Toft and Albarède (1997) have been used along with the corresponding zircon age.

(Figs. 9, 10). Rocks of the studied suite show a variable degree of fractionation, as it is observed particularly in the basic group compositions which show high SiO_2 (> 51%) and low MgO (< 5.1%), Ni (< 160 ppm) and Cr (< 150 ppm) contents (Fig. 10; Table 2). The study of major and trace element Harker diagrams is in part hampered by the presence of the ~13% SiO_2 compositional gap and the underrepresentation of the acid members (Fig. 10). Nevertheless, patterns of possible lines of descent are still shown in several elements in these and other bivariate diagrams using a different proxy for differentiation (e.g. MgO and Zr, not shown). For major elements, this is the case of FeO_t, MgO and CaO, which show a decreasing behavior with increasing differentiation, and K_2O, which increases along with

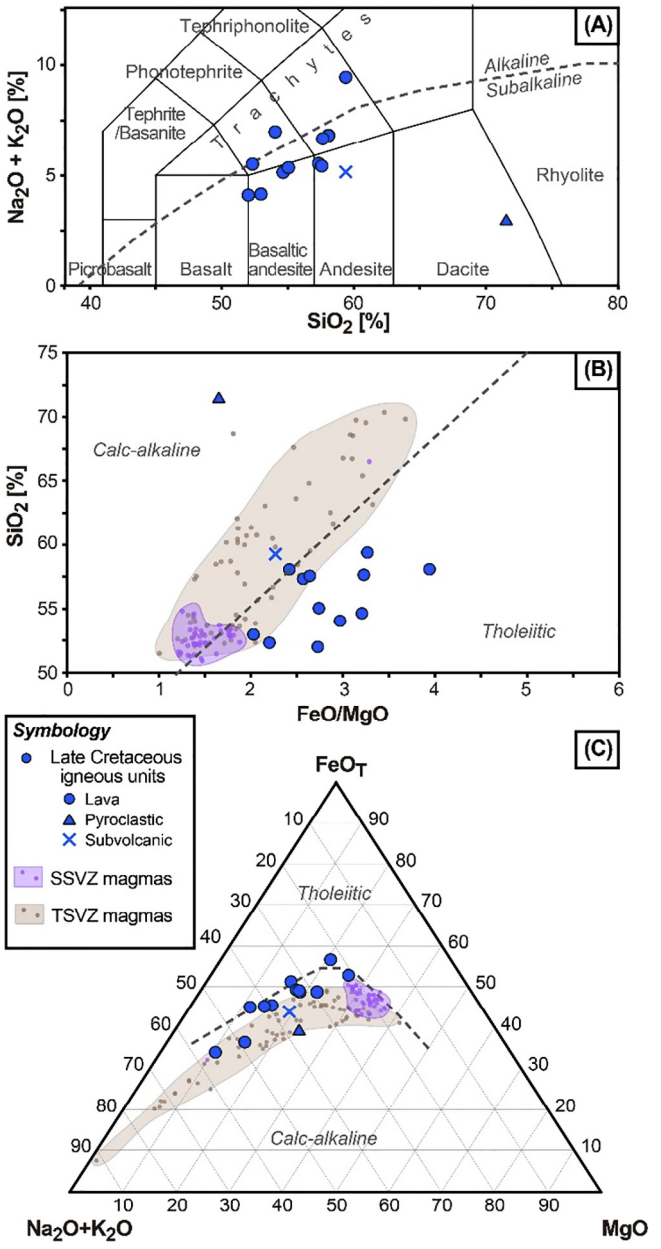

Fig. 9. General compositional features of igneous rocks from the Plan de los Yeuques Formation. Shown diagrams correspond to: (A) TAS, (B) FeO/MgO ratio vs. %SiO_2 and (C) AFM, with magmatic series subdivisions respectively after Irvine and Baragar (1971), Miyashiro (1974) and Kuno (1966). In (B) and (C) the field defined by stratovolcano lavas from the current Andean Southern Volcanic Zone (SVZ) is included as reference. The latter has been grouped in the transitional (TSVZ) and southern (SSVZ) segments, and the data has been taken from Hickey-Vargas et al. (1986), Futa and Stern (1988), Hildreth and Moorbath (1988) and Holm et al. (2014).

differentiation (Fig. 10). A compatible behavior is also seen for the trace elements Sc, Co and V, while some LILE (Ba, Rb) and HFSE (Y, Zr, Hf and LREE) show an incompatible behavior (Fig. 10).

In terms of REE composition all samples show an enriched signature, ranging between 7 and 70 times the chondritic value, with a preferential enrichment of LREE over HREE (Fig. 11). In the chondrite-normalized diagram of Fig. 11 all samples have been plotted together, but they have been grouped according to SiO_2 wt% contents in three: (1) 51–57% (n = 7), (2) 57–60% (n = 6), (3) 71% (n = 1). As seen in this diagram, the two former groups of the more basic samples display mostly subparallel patterns, which become increasingly enriched with differentiation, and an absence of discernible Eu anomalies. Compared to the latter groups, the most differentiated sample (SiO_2 = 71%) is accordingly more enriched in the LREE and HREE but shows a significant depletion in MREE and a marked Eu anomaly (Fig. 11). For the two more basic groups, the patterns displayed suggest a cogenetic relation through crystal fractionation processes of low-pressure mineralogy. This is also supported by the behavior they describe for compatible elements in Harker diagrams and the primary major mineralogy present in these rocks, namely olivine, pyroxene and plagioclase. Respect to the latter groups, the REE pattern of the most differentiated sample can also be explained by further differentiation of the mentioned mineral phases but incorporating plagioclase and amphibole in addition, as it is indeed supported by their modal presence in the acid members of the suite. Even though the hypothesis of a cogenetic relation between the basic and acid members is obscured by the observed compositional gap, this is complimentarily supported by the similarities in terms of Nd and Hf isotopic composition of both groups (see the following). Finally, the absence of fractionation in HREE in all samples disregards the involvement of garnet in their genesis, either as a fractionating phase or as present in the magmatic source.

In a multielement spider diagram, normalized to N-MORB (Pearce, 1983), studied samples show the typical features of arc-related igneous rocks, namely a preferential enrichment of LILE over HFSE and a marked Nb-Ta through (Fig. 11). The more basic groups show subparallel patterns also supporting a cogenetic relation through crystal fractionation from the less differentiated compositions. A compatible behavior can be inferred from elements as Sr, TiO_2, Ni and Cr, while the rest show variable degrees of incompatibility (Fig. 11). Respect to these groups, the most differentiated sample shows a similar behavior but incorporating into the compatible elements Ba, P_2O_5 and Sm, which agrees with petrographic evidence supporting the fractionation of amphibole and apatite in the acid members of the suite (Fig. 11). As seen in this diagram, in particular for the less differentiated samples, the enrichment of LILE over HFSE along with the similar concentrations of the conservative HFSE Nb, Ta, Zr, Hf, Y and Yb (sensu Pearce, 1983) suggest a derivation from a spinel lherzolite mantelic source similar to that of N-MORB metasomatized by a subduction component.

In terms of Sr-Nd isotopic composition the studied suite shows a restricted signature and a juvenile character, with values for the isotopic ratios of $\varepsilon_{Nd}(i)$ between +3.3 and +4.0 and $^{87}Sr/^{86}Sr(i)$ between 0.7039 and 0.7040 (Table 3). Such signature is within the mantle array and more evolved than that of the N-MORB (Fig. 12). Analyzed samples cover a range of SiO_2 contents between ~52 and 58% and isotopic ratios show no patterns of variation against this parameter, Nd or Sr contents. Hf isotopic composition was determined in the zircon crystals analyzed for radiometric determinations, samples which correspond to two vitric tuffs and a lithic lapilli tuff of dacitic compositions. All samples show a similar and restricted range of initial Hf isotopic ratios, with values of $\varepsilon_{Hf}(i)$ between +6.6 and +10.4 indicating also a juvenile signature (Fig. 12; Table 4). The isotopic determinations made for the more basic (Sr-Nd) and the acid (Hf) members of the studied series are not directly comparable, however this can be broadly approached from the akin behavior shown by the Hf and Nd systems in which $\varepsilon_{Hf} \approx 1.36 * \varepsilon_{Nd} + 3.0$ (Vervoort and Blichert-Toft, 1999). According to this relation the calculated $\varepsilon_{Hf}(i)$ for the more basic members varies between +7.6 and +8.5, a range that is fully contained in that defined by the $\varepsilon_{Hf}(i)$ of the acid members (+6.6 to +10.4). This supports that there is a cogenetic relation between both and also that crustal contamination is not a significant process occurring throughout magmatic differentiation.

Further inferences about the magma genetic processes and its framing conditions can be drawn by comparing the geochemical and isotopic characteristics of the studied series against those of the currently active Andean Southern Volcanic Zone (SVZ; ~33–46°S). This has been classically divided into three segments on the basis of the geologic frame and the particular petrologic and geochemical

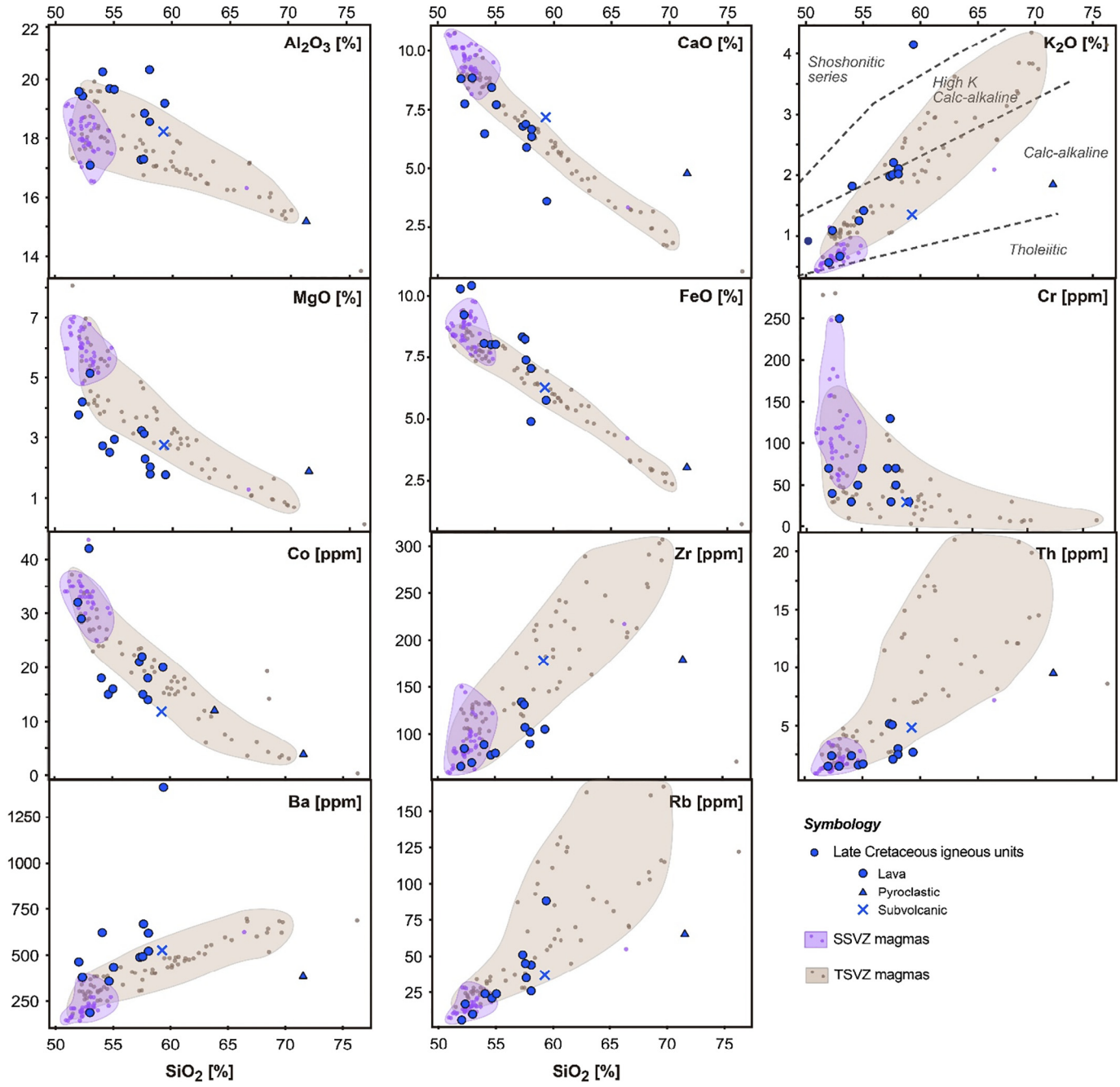

Fig. 10. Selected major and trace element Harker diagrams for igneous rocks of the Plan de los Yeuques Formation. Fields defined by the current Andean Southern Volcanic Zone magmas (SVZ) as in Fig. 1.

characteristics of their corresponding magmas, both features that have been shown to be intimately related (e.g. Hildreth and Moorbath, 1988; Stern, 2004). Among the main characteristics, SVZ magmas form and evolve under a continuously decreasing crustal thickness southwards (Tassara and Echaurren, 2012) and show marked differences in the nature and amount of crustal components involved in their genesis (e.g. Hildreth and Moorbath, 1988; Stern, 2004). For comparison, in the different chemical diagrams presented the composition defined by the SVZ has been included accordingly for the Northern (NSVZ; ~33–34.4°S), Transitional (TSVZ; ~34.4–37°S) and Southern (SSVZ; ~37–42°S) segments (Fig. 1A). In terms of chemical and isotopic characteristics, the studied series shows numerous similarities to magmas from the SSVZ and differences against those from the TSVZ and NSVZ. This is particularly the case for the Sr-Nd isotopic composition, where the signature of the studied suite is totally contained within the juvenile range defined by the SSVZ and is in particular more juvenile than the current magmas hosted at the same latitude (~35°S, TSVZ; Fig. 12). Such feature suggests similar geochemical components and/or sources involved in the genesis of both magmatic suites and also supports the low involvement of crustal contamination processes for the studied rocks. In terms of chemical composition, and compared at similar differentiation degrees (e.g. SiO_2 and MgO wt% contents), the studied suite shows contents and patterns of HFSE and HREE similar to the SSVZ which are in turn distinctly different from the other SVZ segments (Fig. 13). However, a marked compositional difference against the SSVZ magmas is seen in: (1) lower MgO contents, which is

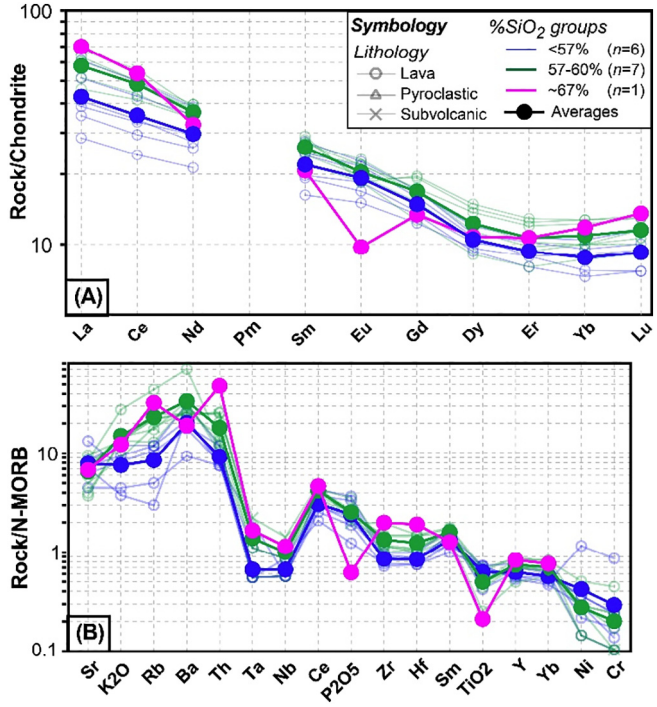

Fig. 11. Multielement diagrams of igneous rocks from the Plan de los Yeuques Formation. (A) REE concentrations normalized to chondrite (Nakamura, 1974), and (B) spider multielement plot normalized to N-MONB (Pearce, 1983).

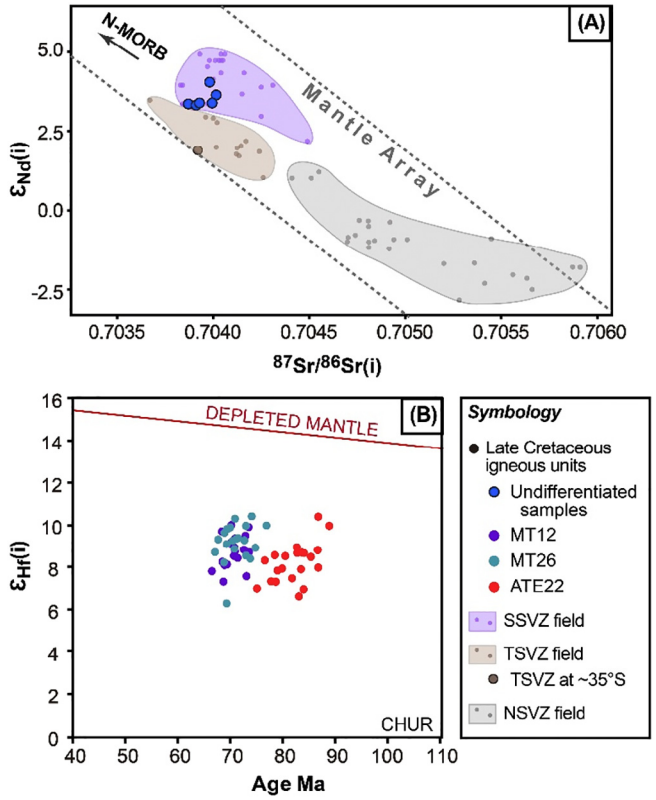

Fig. 12. Sr, Nd and Hf isotopic composition of igneous rocks from the Plan de los Yeuques Formation. (A) $\varepsilon_{Nd}(i)$ vs. $^{87}Sr/^{86}Sr(i)$ and (B) $\varepsilon_{Hf}(i)$ vs. age. Geochemical reservoirs included for reference correspond to (A) Mantle Array (Wilson, 1989) and (B) Chondritic (CHUR; Blichert-Toft and Albarède, 1997) and Depleted Mantle (Vervoort and Blichert-Toft, 1999). Fields defined by the current Andean Southern Volcanic Zone magmas (SVZ) as in Fig. 1 for the Southern (SSVZ) and Transitional (TSVZ) segments. For the Northern segment data is also included from Stern et al. (1984).

also observed for other compatible elements (Sc, V, Cr, Co, Ni; Fig. 10) and (2) higher FeO_t, LILE and LREE contents (Fig. 13). Along with the previous observations, this results in differences in trace element ratios commonly used to infer components and/or processes involved in magma genesis (e.g. LREE/HREE, LILE/HFSE, LREE/LILE).

In terms of magma genetic processes, and as suggested by the similar isotopic signature, the studied suite can be easily derived from SSVZ parental magmas. These have been recently characterized by Hickey-Vargas et al. (2016) from basalts of small eruptive centers (SEC) nearby the Villarrica stratovolcano (~39°S; ~30–35 km crustal thickness). Such basalts are among the most primitive compositions reported for SSVZ (MgO contents up to 14%) and, according to the authors, they derive from mantle melting processes with little interaction with the crust. Two main compositional groups are distinctive among SEC, Type 1 and Type 2, with the latter showing comparatively higher LREE, lower LILE/LREE and LILE/HFSE, and lower ε_{Nd} for a range in $^{87}Sr/^{86}Sr$ ratios. According to Hickey-Vargas et al. (2016), Type 1 basaltic magmas form by melting of the ambient actively subduction-modified asthenosphere, while Type 2 incorporate melts of pyroxenite residing in the supra-subduction zone mantle lithosphere which has been modified by magmatism of earlier episodes of subduction. Compared to these compositional poles, the studied suite shows the same isotopic signature as the Type 2 basalts, yet in terms of many of the major and minor elements its characteristics are similar to Type 1 basalts or to a mixing between both types (Fig. 14). Several simple mixing scenarios between extreme members of both parental compositions can reproduce the isotopic signature of the studied suite, specifically between 80–40% Type 1 and 20–60% Type 2, and also its main compositional features (Fig. 14). The latter however shows minor misfits, in particular for compatible elements, which can be easily accommodated by crystal fractionation processes of early mafic phases. This in turn agrees with the comparatively more fractionated nature shown by the studied suite basalts (Fig. 14).

7. Discussion

7.1. Regional correlations of the BRCU and paleogeographic implications

Based on lithological aspects, stratigraphic position and fossil content, previous works have proposed that the BRCU correlated with the early Cenomanian-Campanian Neuquén Group in Argentina (~100–75 Ma; Fig. 15A; Charrier et al., 1996; Mescua et al., 2013; Fennell et al., 2015). Our determination of a latest Cenomanian-early Campanian (~95–80 Ma) depositional age for the BRCU supports such correlation, yet the detrital zircon patterns of both units markedly differ indicating both different source areas and evolution during deposition (Fig. 15B).

Detrital zircons ages for the BRCU show only a Cretaceous component (Fig. 15B), which can be derived either from: (i) the Cretaceous volcanic and intrusive arc rocks located west of the study area, along the Coastal Cordillera (Fig. 1B), or (ii) the Lower Cretaceous sedimentary sequences of the Neuquén basin as a recycled component (Fig. 1B; Tunik et al., 2010; Aguirre-Urreta et al., 2011; Di Giulio et al., 2012, 2016; Balgord and Carrapa, 2014). Detrital zircon ages of the Neuquén Group vary according to both stratigraphic (Tunik et al., 2010; Di Giulio et al., 2012) and geographic position (cf. Fennell et al., 2015). The lower Neuquén Group (cf. Balgord and Carrapa, 2014) is characterized by a Jurassic-Early Cretaceous arc component (< 200 Ma) and a minor Early Triassic-late Devonian component (200–400 Ma; Fig. 15B). In turn, the middle and upper Neuquén Group (Fig. 15B) exhibit only components with Early Triassic-late Devonian (200–400 Ma) and cratonic (> 400 Ma) ages (Fennell et al., 2015). The

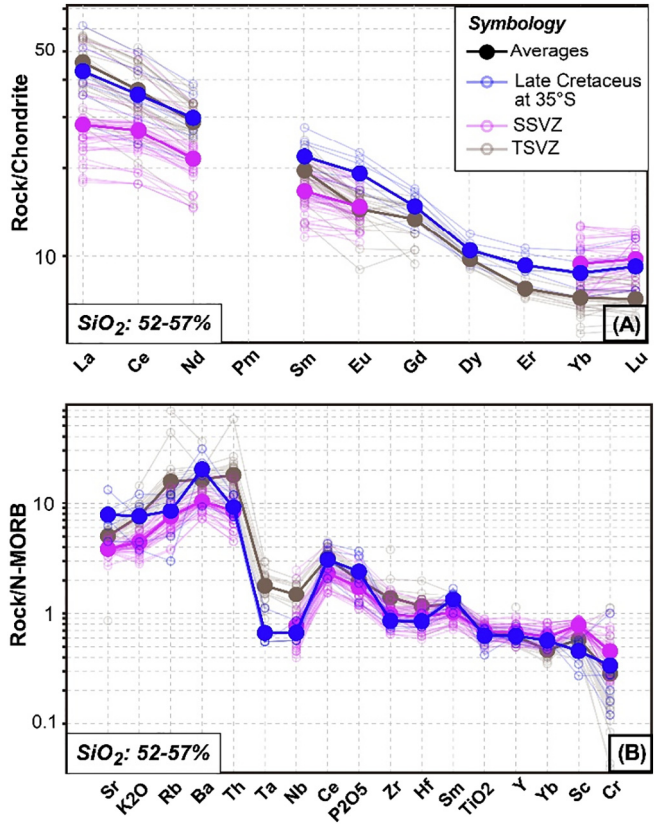

Fig. 13. Multielement diagrams for basaltic andesite compositions comparing the signature of the Plan de los Yeuques Formation against those defined by the Transitional and Southern segments of the current Andean SVZ (see Fig. 1 for references). (A) REE concentrations normalized to chondrite (Nakamura, 1974), (B) spider multielement plot normalized to N-MONB (Pearce, 1983).

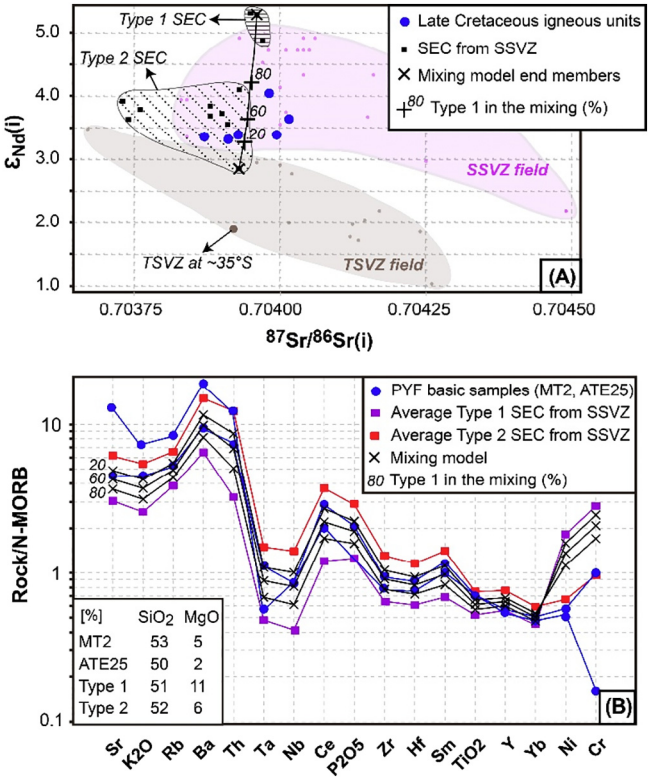

Fig. 14. Simple mixing models between Type 1 and Type 2 SEC (small eruptive cones) end members reproducing the isotopic and chemical signature of volcanic rocks from the Plan de los Yeuques Formation. (A) $\varepsilon_{Nd}(i)$ vs. $^{87}Sr/^{86}Sr(i)$, mixing end members correspond respectively to the highest and lowest values of ε_{Nd} for the Type 1 SEC and the low-$^{87}Sr/^{86}Sr$ Type 2 SEC. (B) Spider multielement plot normalized to N-MONB (Pearce, 1983), mixing end members correspond to average Type 1 and Type 2 SEC, the two most basic compositions of the Plan de los Yeuques Formation are also displayed (samples MT2 and MT6). SEC compositions taken from Hickey-Vargas et al. (2016). See the main text for further details.

former matches the ages of the Neuquén basin basement rocks and thus evidences a provenance either from the east or west of the basin depocenter. In turn, the cratonic components are related to rocks specifically located to the east of the Neuquén depocenter (Fennell et al., 2015). Both source components, located to the east of the study area, are not recognized in the BRCU detrital zircon spectrum which evidences a null sediment supply from them during its deposition. This strongly suggests a different paleogeographic setting for deposition of the Neuquén Group and the BRCU.

The absence of detrital zircons < 100 Ma in the upper Neuquén Group has been interpreted as resulting from the growth of the fold and thrust belt limiting to the west the Cretaceous foreland basin, therefore inhibiting the sediment supply from the Cretaceous magmatic arc located in the current Coastal Cordillera (Fig. 1B; e.g. Fennell et al., 2015). Moreover, the lack of such component in the Neuquén Group has also been ascribed to an inferred decline in the arc activity between ca. 100 and 85 Ma (Fennell et al., 2015; Balgord, 2017). Our detrital zircon data for the BRCU deposits shows a continuous record between 120 and 85 Ma (Fig. 15B), thus supporting the topographic barrier hypothesis. Thereby, a positive relief separating the BRCU and Neuquén Group depocenters would explain the differences in the sources areas shown by these units. This barrier would be part of the Late Cretaceous fold and thrust belt involving the Late Jurassic-Early Cretaceous sedimentary sequences of the Neuquén basin (Fig. 16A). Related to such system, the ENE-WSW oriented structures along the Vergara valley could be the result of the structuring of the fold and thrust belt in the study region and the evidence for a previous deformation event. This is supported by the evidence reported of the Late Cretaceous deformation immediately to east of the study area (Mescua et al., 2013). Overall, the proposed configuration agrees well with the recycling of early Cretaceous sedimentary deposits as a source of the detrital zircons of the BRCU (Figs. 5A and 15B).

Differences in the zircon provenance areas through the Neuquén Group units were interpreted by Fennell et al. (2015) as reflecting its position inside of a foreland basin system (sensu DeCelles and Giles, 1996). In their model, the western outcrops of the Neuquén Group correspond to deposits accumulated in the wedge-top position while the eastern outcrops would represent the foredeep depocenter (Fig. 16A). The BRCU, cropping out to the west of the Neuquén Group (Fig. 1B), would have deposited under this configuration in the wedge-top depozone of the Late Cretaceous foreland basin system. Similarly, Mescua et al. (2013) proposed a paleogeographic model where the BRCU and Neuquén Group deposition began simultaneously in the wedge-top but after being separated by the growth of the fold and thrust belt (Fig. 16A). This model implies a disconnection of the BRCU depocenter with the rest of the foreland basin system to the east and agrees with both the similar deposition age and the differences in the detrital zircon patterns of the mentioned units (Fig. 15B). These arguments indicate that whereas the BRCU depocenter evolved probably as a disconnected piggyback basin (e.g. Beer et al., 1990; Talling et al., 1995; Ori and Friend, 1984), the Neuquén Group accumulated in the connected wedge-top and foredeep depocenters that developed to the east of the study area (Fig. 16A; Fennell et al., 2015).

7.2. The Late Cretaceous magmatic arc: Plan de los Yeuques Formation

Deposits of the Plan de los Yeuques Formation overly the BRCU in

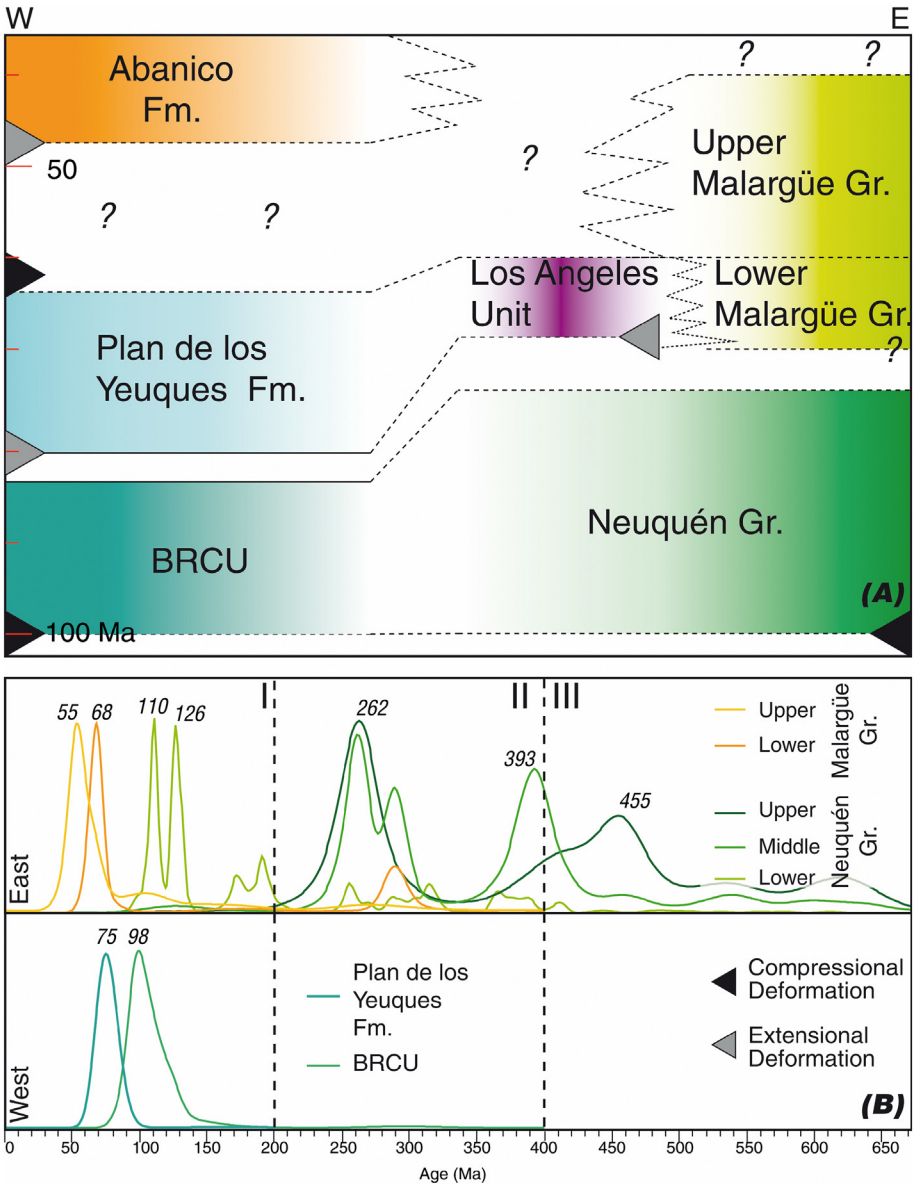

Fig. 15. (A) Chronostratigraphic relations between units of western and eastern Andean slope during the Late Cretaceous-early Paleocene at ~35°S. Lower and Upper Malargüe groups after Balgord and Carrapa (2014). (B) Comparative plot of kernel density estimator for detrital zircon U-Pb ages, this includes the Late Cretaceous deposits of the Neuquén foreland basin system, separated for the western and eastern slope of the Southern Central Andes. Ages for the BRCU and Plan de los Yeuques Formation from this work, and those for Neuquén and Malargüe groups are compiled from Tunik et al. (2010), Di Giulio et al. (2012, 2016), Fennell et al. (2015), Balgord (2016) and Horton and Fuentes (2016). The division of the Neuquén and Malargüe groups is according to Balgord (2016). Jurassic-Cretaceous magmatic-arc (I), Early Triassic-late Devonian (II) and Cratonic (III) sources are shown. Ages for the Los Ángeles Unit are taken from Fennell et al. (2017) and Iannelli et al. (2018).

an apparent concordant contact that records a depositional gap of < 6 m.y., thus both units configure an almost continuous record throughout the Late Cretaceous to the earliest Paleocene in the area. Noticeably, such contact marks a sharp change in the geologic setting, passing from the sedimentary deposits of the BRCU series to the predominantly volcanic nature of the Plan de los Yeuques Formation. This latter feature, along with the arc-like signature of the igneous products, indicate that the Plan de los Yeuques Formation represents the coeval magmatic arc in the area, an episode that extended at least between early Campanian and Danian (~80–63 Ma; Fig. 15A). The establishment of this arc follows from an eastward migration of the magmatic loci, as evidenced by immediately older igneous rocks at the same latitude which are exposed nearly 50 km to the west, in the Central Depression, as a series of felsic plutonic units of 95–83 Ma (Fig. 1A, B; Contreras and Schilling, in press).

Igneous products of the Plan de los Yeuques Formation show a series of compositional and mineralogical characteristics that indicate a predominantly low pressure evolution of the corresponding magmas. This is evidenced in the low pressure mineralogical assemblages which dominate both the fractionation processes and the inferred source composition. Regarding the latter, it is in addition remarkable that the studied suite shows compositional and isotopic characteristics coherent with a derivation form standard parental magmas of the current SSVZ. This is also followed by an almost null involvement of crustal contamination processes through latter differentiation, which in turn arguments for a fairly fast transit of magmas throughout the crust while ascending from the source to upper crustal levels. All this evidence indicates that the formation and latter evolution of the Plan the los Yeuques magmas were framed by a normal to thin crust of 30–35 km thick, similarly to the current SSVZ setting where the crust thins progressively from ~35 km from 38°S southwards (e.g. Tassara and Echaurren, 2012).

A setting under extensional conditions for the arc region throughout deposition of the Plan de los Yeuques Formation is evidenced in the synsedimentary normal faulting recorded in its outcrops. The composition of the corresponding magmas and the setting inferred from them are coherent with such tectonic conditions, and they also place constraints on the paleogeographic configuration upon which the evolution of the area developed. According to the proposed models, the Plan de los Yeuques Formation would have deposited along the hinterland of the Cenomanian-Campanian orogen over a thickened crust after the early Late Cretaceous compressive event (Fig. 16B; cf. Balgord and Carrapa,

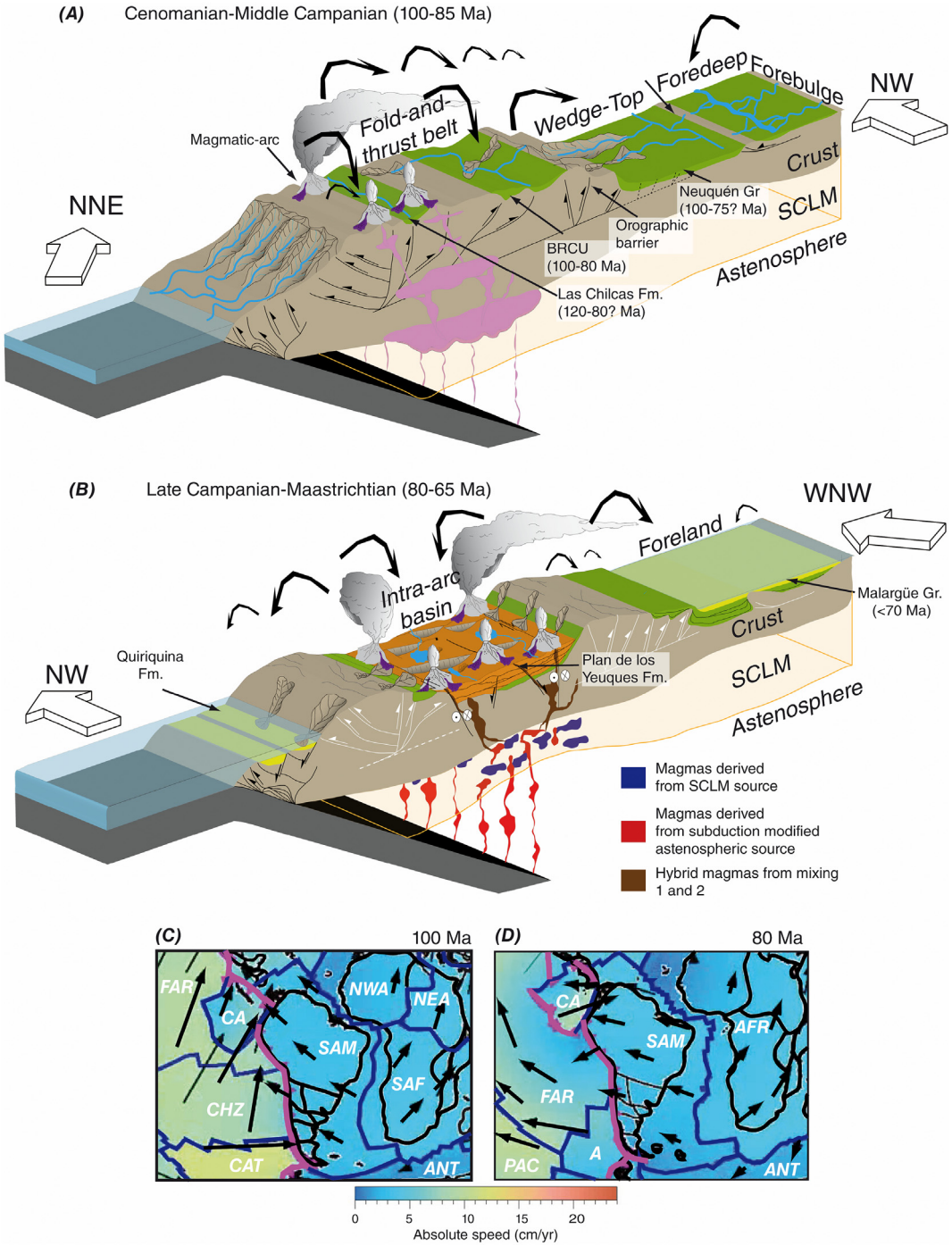

Fig. 16. Paleogeographic reconstruction of the Late Cretaceous evolution of the Andean margin at ~35°S. In (A) and (B) schematic block diagrams summarize the evolution proposed in this work (figures not to scale; see the main text further details). SCLM: Subcontinental Lithospheric Mantle. (C) and (D) display the reconstruction of absolute plate velocities and motion directions of the South American Plate after Müller et al. (2016). The colors and vector lengths indicate plate speed and vector azimuths and represent absolute plate motion directions. Abbreviations: A: Aluk Plate; AFR: African Plate; ANT: Antarctic Plate; CA: Caribbean Plate; CAT: Catequil Plate; CHZ: Chasca Plate; FAR: Farallon Plate; NEA: northeast African Plate; NWA: northwest African Plate; PAC: Pacific Plate; SAF: South African Plate; SAM: South American Plate.

2014; Tunik et al., 2010). However, given the setting inferred from magmas of the Plan de los Yeuques Formation, such crustal thickening either proceeded no further than up to 40 km thickness or was latter attenuated by a thinning process after the orogeny.

The bimodal volcanic suite of the Plan de los Yeuques Formation could also represent a feature resulting from a magmatic evolution under extensional conditions. Worldwide, the association of both features in different tectonic settings is common, although not exclusive, and several models have been proposed to explain the bimodal character of magmatism under extensional conditions. Throughout the evolution of the Andean margin this association has also been frequently recognized, as during the Permo-Triassic (see Maksaev et al., 2014 and references therein) and Early Cretaceous times (see Charrier et al., 2007 and references therein), and in the early stages of the Abanico rift basin event during middle Eocene-Oligocene times (Nyström et al., 2003; Fuentes, 2017). For the Plan de los Yeuques

Formation, a first order observation is the equivalent isotopic signature shown by the corresponding acid and basic igneous compositions. This indicates a cogenetic relation between both members of the suite and thus disregards the classic extensional models of bimodal magma genesis that involve two separate sources, crustal and subcrustal sources respectively for the acid and basic magmatic compositions. Even though partly obscured by the 13% SiO_2 compositional gap, volcanic rocks of the Plan de los Yeuques Formation display mineralogical and compositional characteristics that suggest an evolution through crystal fractionation of olivine, pyroxene, magnetite and plagioclase, in the basic members of the suite, incorporating also amphibole and accessory apatite in the acid members of the suite. As shown by Grove and Nolan (1986), the latter assemblage occurs in a cotectic that is nearly horizontal in a temperature-compositional space, which in turn gives way to a large extent of crystallization in a limited temperature interval and thus prompts the rapid formation of silicic liquids along with a compositional gap. Such processes are favored by low pressure crystallization (< 5 kbar) and also proceed along with a drastic increase in the H_2O content of the residual liquid (Grove and Nolan, 1986). Regarding the former, it has to be noted that all the analyzed volcanic rocks of the Plan de los Yeuques Formation are to a lesser or greater extent fractionated. This observation suggests an overall magmatic system where early fractionation processes occur deep in the continental lithosphere and the resulting magmas, still basic in composition, are able to reach upper crustal levels where they either erupt or proceed with further crystallization. Moreover, the fact that the acid members of the studied suite are exclusively represented by pyroclastic rocks reveals an explosive nature of volcanism, this in turn could be related to the increase in the H_2O contents that proceeds along with late crystallization. Altogether, these observations fit both the compositional characteristics of volcanic rocks from the Plan de los Yeuques Formation and the framing setting where they occur, that is a 30–35 km thick crust under extensional conditions.

Summarizing the arguments previously exposed, we envisage the overall tectono-magmatic system represented by the Plan the los Yeuques Formation as follows (Fig. 16B). Early primary magmas would derive from the subduction modified mantle, both from asthenospheric and lithospheric sources similar to those currently sourcing SSVZ Andean magmas. Although melting of the subduction modified asthenospheric source is straightforward in the paradigm of a subduction setting, the involvement of a lithospheric mantle component is more elusive. For melting and incorporating such source two main not exclusive scenarios could be invoked: (i) an increase in temperature due to the heat supplied by ascension and deep stalling of asthenospheric derived magmas, or (ii) decompression melting in response to extensional tectonics and crustal thinning processes. Following the formation of primary magmas, an early stage of differentiation should take place deep in the upper continental lithosphere before fractionated basic magmas reach upper crustal levels. In the latter place, such magmas would either erupt or stall in shallow crustal reservoirs where a rapid crystallization would prompt the generation of the acid members of the suite associated with explosive volcanism. In a whole, the nature, structure and geochemical characteristics determined for the Plan de los Yeuques Formation support the hypothesis of deposition in an intra-arc basin setting where extension and crustal thinning would be responsible of the subsidence in the arc area.

7.3. Implications for the Late Cretaceous Andean tectonic setting

More than a local feature, the extensional setting inferred for the arc region during deposition of the Plan de los Yeuques Formation seems to be of a regional scale. Nearly 76 km southeast of the studied area such conditions are also recorded by the partly coeval series of the Los Ángeles Unit (~65 Ma; Figs. 1B, 15A), in the Argentinean slope of the Andes (~35°30′S; Fennell et al., 2017; Iannelli et al., 2018). At a larger scale, other studies along the Andean margin also support this hypothesis. Between 20° and 27°S, in the western slope of the Andes, several studies have proposed the development of an intra-arc extensional basin system during Late Cretaceous (Blanco et al., 2012; Cornejo and Matthews, 2001; Cornejo et al., 2003; Espinoza et al., 2009; Matthews et al., 2010), a system including the basins of: Cerro Empexa-Challacollo (20°-21°S, Blanco et al., 2012), Quebrada Mala (22°–24°30′S, Marinovic et al., 1996; Marinovic and García, 1999) and Llanta (25°55′–27°S, Cornejo and Matthews, 2001; Cornejo et al., 2003, 2009; Matthews et al., 2010). Extensional conditions were also inferred for the deposition of the volcanic and sedimentary series of the Sierra de Fraga region (~27°S; Mpodozis and Allmendinger, 1993) and to the Lo Valle Formation (~33°S; see Charrier et al., 2007 and references therein). Altogether, this evidence indicates that at least the Andean arc region underwent extensional deformation during the latest Late Cretaceous. Such episode took place after the compressive deformation associated to Peruvian Orogenic phase during early Late Cretaceous (Fig. 16A; Steinman, 1929) and therefore entails regional changes on the orogenic wedge building during this time. Moreover, the evidence of the post-deposition folding along the northern slope of the Tinguiririca valley (Fig. 2) indicate that the Plan de los Yeuques Formation was also affected by both the K-T and Incaic deformational phases. The latter affected the Andean margin between the latest Late Cretaceous to Eocene (e.g. Charrier et al., 2007), and is also recorded in the northward Late Cretaceous volcanic deposits along the western slope of the Andean orogen (Blanco et al., 2012, Cornejo and Matthews, 2001; Cornejo et al., 2003; Espinoza et al., 2009; Matthews et al., 2010).

Several scenarios can be explored to explain the tectonic configuration governing the described Late Cretaceous-earliest Paleocene evolution of the margin. If the earliest Late Cretaceous compression continued until Paleocene, then internal shortening in the rear region of an orogenic wedge could have triggered extension by over-steepening its taper to a supercritical state (Dahlen, 1984; Platt, 1986; Cello and Mazzoli, 1996). This scenario entails thickening by either underplating at the base of the wedge or internal shortening by duplex and crustal ramps within the wedge (e.g. Platt, 1986). There is no substantial data about the Peruvian orogen (architecture, shortening, height or length) along the Andean margin to recognize the occurrence of such processes, however extension in a thickening region by large-scale ramps may seem reasonable for the development of individual core complexes. Although plausible for individual regions, such mechanism is unlikely for the Late Cretaceous extension in the margin when considering that documented localities extend for > 1700 km along strike between 20° and 36°S.

The alternation of extensional and compressional episodes throughout the evolution of the Southern Central Andes is a common feature which has been frequently ascribed to a shallowing-steepening slab model (e.g. Ramos and Folguera, 2005; Kay et al., 2006; Folguera and Ramos, 2011; Spagnuolo et al., 2012; Fennell et al., 2017). This is particularly the case for the Late Cretaceous in the study region, where latest works have proposed a combination of shallowing-steepening slab conditions along with asthenospheric window processes as the parameters governing the coeval evolution recorded in the continental lithospheric plate (e.g. Ramos and Folguera, 2005; Spagnuolo et al., 2012; Fennell et al., 2017; Iannelli et al., 2018). According to these, a slab shallowing stage would have developed due to subduction of the Chasca/Catequil mid-ocean ridge (Fig. 16C; Seton et al., 2012), between ~100 and 80 Ma, which in turn would be responsible for the coeval eastern migration of the arc and deformation. After the extinction of such ridge, at ~80 Ma, the subduction of the Farallon/Antarctic mid-ocean ridge (Fig. 16D; Seton et al., 2012; Müller et al., 2016) would have entailed asthenospheric slab window processes which are ascribed as responsible for the development of extensional conditions

and arc volcanism in the upper plate (Fennell et al., 2017; Iannelli et al., 2018). The data presented in this study supports neither the timing nor the magmatic consequences that this hypothesis of framing tectonic conditions entails. Regarding the first, our data along with that in the region further west, in the Central Depression (Contreras and Schilling, in press), indicate that the ~95–83 Ma magmatic loci did not migrate from the latter location until ~80 Ma, when the Plan de los Yeuques Formation began its deposition in the current western slope of the main Andes. Therefore, this evidence contradicts the proposed ~100–80 Ma slab shallowing event followed by a steepening stage from ~80 Ma onwards in the region. Regarding magmatic processes, firstly it has been shown in the previous discussions that volcanic rocks from the Plan de los Yeuques Formation show compositional characteristics indicating a derivation from standard SSVZ parental magmas. This observation does not support the participation of any particular geochemical component in the magma-genesis, as it could be expected from the involvement of slab window processes occurring in the asthenospheric source. Additional arguments disregarding the latter hypothesis can be drawn by taking into account the characteristics of Andean magmatism less speculatively known to be framed by such setting, that is the Eocene and Mio-Pliocene volcanics formed above the triple junction of the Andean margin at ~46°30′S (e.g. Espinoza et al., 2005, 2008). Here, first order characteristics include an absence of frontal arc volcanism coupled with the extrusion of large volumes of flood basalts in the rear arc region, the latter in addition showing strong OIB-like and juvenile signatures and evidence of derivation from deep mantle sources within the garnet-spinel stability field (~65–70 km). Such features do not agree at all with what it is observed for the Late Cretaceous evolution of the margin at ~35°S, neither in the frontal arc area, represented by the Plan de los Yeuques Formation in Chile, nor in the near rear arc area, represented by the Los Ángeles unit in Argentina (Iannelli et al., 2018). Regarding the igneous products of this latter unit, Iannelli et al. (2018) reported geochemical characteristics showing an arc-like signature but with a significant enrichment. These features were ascribed by the authors to an OIB-like signal related to the development of an incipient slab-window process. A geochemical comparison between igneous rocks of such unit and those of the Plan de los Yeuques Formation reveals indeed a more enriched nature for the former (see Supplementary material item 3), yet this could be easily explained by a lower degree of melting in the mantle source at that locality. Although no isotopic data is available for the Los Ángeles Unit to further support this hypothesys, this is also coherent with its more inland position respect to the frontal arc magmatism represented by the Plan de los Yeuques Formation (Fig. 1B).

Although our data questions the proposed evolution described above, overall plate tectonic configuration during Late Cretaceous-earliest Paleogene times correlates well with the evolution recorded in the upper continental plate. Reconstructions show that the apparent motion between the Chasca-Catequil and South American plates was convergent between ~120 and 80 Ma (Fig. 16C; Müller et al., 2016; Seton et al., 2012), which agrees well with occurrence of the Peruvian phase and the shortening of the western margin of Gondwana (Fig. 16A; e.g. Tunik et al., 2010; Arriagada et al., 2006). A new plate tectonic reorganization occurred at ~80 Ma, which is marked by the ending of the Chasca-Catequil plates subduction and the establishment of the subduction of the Farallon-Aluk plates under South America (Fig. 16D; Müller et al., 2016; Seton et al., 2012). During the latest Cretaceous to early Paleogene, the convergent margin system was characterized by both: (i) a decrease of the trench normal convergence velocity between the subducting Farallon plate and the overriding South American plate (Fig. 16C; Maloney et al., 2013), and (ii) a decrease of the trench normal absolute velocity of the South American plate (Fig. 16D; Maloney et al., 2013). This geodynamic setting should favor the trench retreat (or roll-back process) and thus a diminished plate coupling (cf. Schellart, 2008), therefore leading to an either neutral o extensional regime in the upper plate as it has been proposed for the Neuquén domain in these times (Balgord and Carrapa, 2014; Horton and Fuentes, 2016; Horton, 2018). It is noteworthy that during this period the trench normal absolute velocity of the South American plate decreased but the latter was still moving towards the trench at that time (Fig. 16D; Maloney et al., 2013; Seton et al., 2012; Müller et al., 2016). The continued westward motion of the overriding plate would have inhibited a widespread extension in it as a consequence of the plate decoupling thereby restricting the deformation only to the western region (e.g. Horton, 2018). Overall, this scenario supports the extensional deformation of the hinterland of the earliest Late Cretaceous Andean orogen, a process that would result from the reduced tectonic stress conditions that follows from a plate convergence rate that is lower than the rate of subduction (cf. Schellart, 2008).

8. Summary and conclusions

In the Chilean Andes, at 35°S, the Late Cretaceous-earliest Paleogene Andean evolution is recorded nearly continuously by two stratigraphic units: (i) the BRCU, a predominantly sedimentary series with a Cenomanian-early Campanian age (~95–80 Ma), and (ii) the Plan de los Yeuques Formation, a predominantly volcanic series with a Campanian-Danian age (~80–65 Ma). Their characteristics indicate an evolving paleogeographic configuration dominated respectively by early sedimentation in the rear arc area, to the east of the Cenomanian-Campanian orogen, which was later over imposed by the establishment of the volcanic arc. As indicated by detrital zircon age patterns, the depocenter of the BRCU would have evolved disconnected from that hosting the foreland basin deposits currently represented by the lower to middle units of the Neuquén Group in Argentina. This in turn indicates the existence of a topographic barrier separating both domains, which would be part of the Late Cretaceous fold and thrust belt involving the Late Jurassic-Early Cretaceous sedimentary sequences of the Neuquén basin. Following deposition of the BRCU, the overlying Plan de los Yeuques Formation records the eastern migration into the area of the previous Cenomanian-Campanian magmatic loci at least since ~80 Ma, and a deposition under extensional conditions. Detrital zircon patterns of this unit also show a depocenter disconnected from that hosting the foreland basin deposits represented by the Upper Neuquén and Lower Malargüe groups.

The volcanic deposits of the Plan de los Yeuques Formation show a series of compositional characteristics that indicate an arc-like signature, low pressure formation and fractionation of the related magmas, and an almost null involvement of crustal contamination processes throughout the magmatic evolution. In addition, such compositional characteristics also agree with a derivation from parental magmas as those sourcing the currently active Andean SSVZ. Altogether, these features and the extensional setting where they develop are consistent with an evolution framed by a normal to thin crust of ~30–35 km thickness, similar to that present in the SSVZ area. This inference place constraints on the paleogeographic configuration upon which the evolution of the area developed after the early Late Cretaceous orogenic processes. In this regard, associated crustal thickening must have proceeded no further than up to 40 km or was latter attenuated by a thinning process after the orogeny.

The extensional conditions recorded in the Plan de los Yeuques Formation are also recorded in numerous Late Cretaceous deposits along the Andean margin, thus highlighting its regional character during this period. We hypothesize that the latter is prompted by both: (i) the similar absolute motion of the subducting Farallon plate and the overriding South American plate, and (ii) a higher velocity of the former than that of the latter (e.g. Müller et al., 2016). Overall, this scenario supports an extensional deformation in the hinterland of the Late Cretaceous Andean orogen, a process that would result from the reduced tectonic stress conditions that follows from a plate convergence rate that is lower than the rate of subduction.

Acknowledgments

This work was funded by the Chilean government through the project Fondecyt 11140012 (CONICYT, Chilean national research agency). This is a contribution of the Instituto de Estudios Andinos Don Pablo Groeber (R263). Carefull reviews of Dr. A. Folgurea and Dr. F. Martínez are gratefully acknowledged.

Appendix A. Supplementary data

Supplementary data to this article can be found online at https://doi.org/10.1016/j.tecto.2018.06.009.

References

Aguirre-Urreta, B., Tunik, M., Naipauer, M., Pazos, P., Ottone, E., Fanning, M., Ramos, V.A., 2011. Malargüe Group (Maastrichtian–Danian) deposits in the Neuquén Andes, Argentina: implications for the onset of the first Atlantic transgression related to western Gondwana break-up. Gondwana Res. 19, 482–494.

Arancibia, G., 2004. Mid-cretaceous crustal shortening: evidence from a regional-scale ductile shear zone in the Coastal Range of central Chile (32° S). J. S. Am. Earth Sci. 17, 209–226.

Armas, P., Moreno, C., Sánchez, M.L., González, F., 2014. Sedimentary palaeoenvironment, petrography, provenance and diagenetic inference of the Anacleto Formation in the Neuquén Basin, Late Cretaceous, Argentina. J. S. Am. Earth Sci. 53, 59–76.

Arriagada, C., Cobbold, P.R., Roperch, P., 2006. Salar de Atacama basin: a record of compressional tectonics in the central Andes since the mid-Cretaceous. Tectonics 25, TC1009.

Astaburuaga, D., 2014. Evolución Estructural del límite Mesozoico-Cenozoico de la Cordillera Principal entre 35°30′ y 36°S, Región del Maule, Chile. Departamento de Geología, Universidad de Chile (Ph.D. Thesis, 128 pp.).

Balgord, E., 2016. Triassic to Neogene Evolution of the Andean Retroarc: Neuquén Basin, Argentina. Department of Geosciences, The University of Arizona (Ph.D. Thesis, 177 pp.).

Balgord, E., 2017. Triassic to Neogene evolution of the south-central Andean arc determined by detrital zircon U-Pb and Hf analysis of Neuquén Basin strata, central Argentina (34°S–40°S). Lithosphere 9, 453–462.

Balgord, E., Carrapa, B., 2014. Basin evolution of Upper Cretaceous–Lower Cenozoic strata in the Malargüe fold-and-thrust belt: northern Neuquén Basin, Argentina. Basin Res. 28, 183–206.

Beer, J.A., Allmendinger, R.W., Figueroa, D.E., Jordan, T.E., 1990. Seismic stratigraphy of a Neogene piggyback basin, Argentina. Am. Assoc. Pet. Geol. Bull. 74, 1183–1202.

Blanco, N., Vázquez, P., Sepúlveda, F.A., Tomlinson, A.J., Quezada, A., Ladino, M., 2012. Levantamiento geológico para el fomento de la exploración de recursos minerales e hídricos de la Cordillera de la Costa. In: Depresión Central y Precordillera de la Región de Tarapacá (20°–21°S). Sernageomin, IR-12-50, Santiago (246 pp.).

Blichert-Toft, J., Albarède, F., 1997. The Lu-Hf isotope geochemistry of chondrites and the evolution of the mantle-crust system. Earth Planet. Sci. Lett. 148, 243–258.

Boyce, D., 2015. Modelo de evolución tectónica y paleogeográfica del margen Andino en Chile Central durante el Cretácico Medio - Tardío: el registro estructural y sedimentario en la Formación Las Chilcas. Departamento de Geología, Universidad de Chile (M.Sc. Thesis, 215 pp.).

Case, A.M., López-Escobar, L., Danieli, J.C., Schalamuk, I.B.A., 2008. Butalón igneous rocks, Neuquén, Argentina: age, stratigraphic relationships and geochemical features. J. S. Am. Earth Sci. 26, 188–203.

Cello, G., Mazzoli, S., 1996. Extensional processes driven by large-scale duplexing in collisional regimes. J. Struct. Geol. 18, 1275–1279.

Charrier, R., Wyss, A.R., Flynn, J.J., Swisher, C., Norell, M.A., Zapata, F., McKenna, M.C., Novacek, M.J., 1996. New evidence for Late Mesozoic-Early Cenozoic evolution of the Chilean Andes in the upper Tinguiririca Valley (35′S), central Chile. J. S. Am. Earth Sci. 9, 393–422.

Charrier, R., Pinto, L., Rodríguez, M.P., 2007. Tectonostratigraphic evolution of the Andean orogen in Chile. In: Moreno, T., Gibbons, W. (Eds.), The Geology of Chile. The Geological Society, London, pp. 21–114.

Charrier, R., Baeza, O., Elgueta, S., Flynn, J.J., Gana, P., Kay, S.M., Muñoz, N., Wyss, A.R., Zurita, E., 2002. Evidence for Cenozoic extensional basin development and tectonic inversion south of the flat-slab segment, southern Central Andes, Chile (33°-36°S.L.). J. S. Am. Earth Sci. 15, 117–139.

Charrier, R., Ramos, V.A., Tapia, F., Sagripanti, L., 2014. Tectono-stratigraphic evolution of the Andean Orogen between 31 and 37°S (Chile and Western Argentina). In: Sepúlveda, S.A., Giambiagi, L.B., Moreiras, S.M., Pinto, L., Tunik, M., Hoke, G.D., Farías, M. (Eds.), Geodynamic Processes in the Andes of Central Chile and Argentina. Geological Society, London, Special Publications, vol. 399. pp. 13–61.

Cingolani, C.A., 2017. San Rafael Block geological map compilation. In: Cingolani, C.A. (Ed.), Pre-Carboniferous Evolution of the San Rafael Block, Argentina, pp. 257–264.

Contreras, J.P., Schilling, M., 2018. Geología del área San Fernando - Curicó. In: Carta Geológica de Chile, Serie Geológica Básica. Servicio Nacional de Geología y Minería, Santiago (in press, 50 pp.).

Cornejo, P., Matthews, S., 2001. Evolution of magmatism from the uppermost Cretaceous to Oligocene, and its relationship to changing tectonic regime. In: The Inca de Oro-El Salvador Area (Northern Chile). III South American Symposium on Isotope Geology, Pucón, Proceedings, vol. S6. pp. 558–561.

Cornejo, P., Matthews, S., Pérez de Arce, C., 2003. The "K-T" compressive deformation event in northern Chile (24–27°S). In: X Congreso Geológico Chileno, Concepción, Concepción, Digital Abstracts, vol. ST1. pp. 1–13.

Cornejo, P., Mpodozis, C., Rivera, O., Matthews, S., 2009. Carta Exploradora, Regiones de Antofagasta y Atacama. In: Carta Geológica de Chile, Serie Geología Básica, vol. 119 Servicio Nacional de Geología y Minería, Santiago (100 pp.).

Dahlen, F.A., 1984. Noncohesive critical Coulomb wedges: an exact solution. J. Geophys. Res. 89, 10125–10133.

DeCelles, P., Giles, K.A., 1996. Foreland basin system. Basin Res. 8, 105–123.

Di Giulio, A., Ronchi, A., Sanfilippo, A., Tiepolo, M., Pimentel, M., Ramos, V.A., 2012. Detrital zircon provenance from the Neuquén Basin (south-central Andes): Cretaceous geodynamic evolution and sedimentary response in a retroarc-foreland basin. Geology 40, 559–562.

Di Giulio, A., Ronchi, A., Sanfilippo, A., Balgord, E., Carrapa, B., Ramos, V.A., 2016. Cretaceous evolution of the Andean margin between 36°S and 40°S latitude through a multi-proxy provenance analysis of Neuquén Basin strata (Argentina). Basin Res. 29, 284–304.

Dickinson, W.R., Gehrels, G.E., 2009. Use of U-Pb ages of detrital zircons to infer maximum depositional ages of strata: a test against a Colorado Plateau Mesozoic database. Earth Planet. Sci. Lett. 288, 115–125.

Espinoza, F., Morata, D., Pelleter, E., Maury, R.C., Suarez, M., Lagabrielle, Y., Polvé, M., Bellon, H., Cotten, J., De la Cruz, R., Guivel, C., 2005. Petrogenesis of the Eocene and Mio-Pliocene alkaline basaltic magmatism in Meseta Chile Chico, southern Patagonia, Chile: evidence for the participation of two slab windows. Lithos 82, 315–343.

Espinoza, F., Morata, D., Polvé, M., Lagabrielle, Y., Maury, R.C., Guivel, C., Cotten, J., Bellon, H., Suárez, M., 2008. Bimodal back-arc alkaline magmatism after ridge subduction: Pliocene felsic rocks from Central Patagonia (47°S). Lithos 101, 191–217.

Espinoza, F., Cornejo, P., Matthews, S., 2009. Geochronology of Late Cretaceous-Early Cenozoic Magmatism in Northern Chile (24°30′–26° S). vol. 21. Latein Amerika Kolloquium (LAK), Göettingen, pp. 88–92.

Farías, M., Comte, D., Charrier, R., Martinod, J., Tassara, A., Fock, A., 2010. Crustal-scale structural architecture of the central Chile Andes based on 3D seismic tomography, seismicity, and surface geology: implications for mountain building in subduction zones. Tectonics 29, TC3006.

Fennell, L., Folguera, A., Naipauer, M., Gianni, G., Rojas Vera, E., Bottesi, G., Ramos, V.A., 2015. Cretaceous deformation of the southern Central Andes: synorogenic growth strata in the Neuquén Group (35°30′–37°S). Basin Res. 29, 51–72.

Fennell, L., Iannelli, S., Folguera, A., Encinas, A., Sagripanti, L., Colavitto, B., Valencia, V., 2017. Interrupciones extensionales en el desarrollo de la Faja Plegada y Corrida de Malargüe (36°S). In: XX Congreso Geológico Argentino, San Miguel de Tucumán, Digital Abstracts, vol. S12. pp. 88–90.

Folguera, A., Ramos, V.A., 2011. Repeated eastward shifts of arc magmatism in the Southern Andes: a revision to the long-term pattern of Andean uplift and magmatism. J. S. Am. Earth Sci. 32, 531–546.

Franchini, M., López-Escobar, L., Schalamuk, I.B.A., Meinert, L., 2003. Magmatic characteristics of the Paleocene Cerro Nevazón region and other Late Cretaceous to Early Tertiary calc-alkaline subvolcanic to plutonic units in the Neuquén Andes, Argentina. J. S. Am. Earth Sci. 16, 399–421.

Fuentes, C., 2017. Los Estratos del Cordón de los Ratones del río Maipo (33°66′S, 70°39′W): petrografía, geoquímica, e implicancias en la evolución del Paleógeno en Chile Central. Departamento de Geología, Universidad de Chile (Geologist Thesis, 90 pp.).

Futa, K., Stern, C.R., 1988. Sr and Nd isotopic and trace element compositions of Quaternary volcanic centers of the southern Andes. Earth Planet. Sci. Lett. 88, 253–262.

Gana, P., Wall, R., 1997. Evidencias geocronológicas 40Ar/39Ar y K-Ar de un hiatus Cretácico Superior-Eoceno en Chile Central (33–33°30′S). Andean. Geology 24, 145–163.

Gómez-Tuena, A., Mori, L., Goldstein, S., Pérez-Arvizu, O., 2011. Magmatic diversity of western Mexico as a function of metamorphic transformations in the subducted oceanic plate. Geochim. Cosmochim. Acta 75, 213–241.

Gómez-Tuena, A., LaGatta, A., Langmuir, C.H., Goldstein, S.L., Ortega-Gutiérrez, F., Carrasco-Núñez, G., 2003. Temporal control of subduction magmatism in the Eastern Trans-Mexican Volcanic Belt: mantle sources, slab contributions and crustal contamination. Geochem. Geophys. Geosyst. 4. http://dx.doi.org/10.1029/2003GC000524.

González, O., Vergara, M., 1962. Reconocimiento geológico de la Cordillera de los Andes entre los paralelos 35° y 38°S. vol. 24 Instituto de Geología, Universidad de Chile, Santiago (70 pp.).

Gripp, A.E., Gordon, R.G., 2002. Young tracks of hotspots and current plate velocities. Geophys. J. Int. 150, 321–361.

Grove, T.L., Nolan, J.M.D., 1986. The evolution of young silicic lavas at Medicine Lake Volcano, California: implications for the origin of compositional gaps in calc-alkaline series lavas. Contrib. Mineral. Petrol. 92, 281–302.

Haschke, M., Siebel, W., Günther, A., Scheuber, E., 2002. Repeated crustal thickening and recycling during the Andean orogeny in north Chile (21°–26°S). J. Geophys. Res. 107, 2019.

Hickey-Vargas, R., Frey, F.A., Gerlach, D.C., 1986. Multiple source for basaltic arc rocks from the Southern Volcanic Zone of the Andes (34°-41°S): trace element and isotopic evidence for contributions from subducted crust, mantle, and continental crust. J. Geophys. Res. 91, 5963–5983.

Hickey-Vargas, R., Sun, M., Holbik, S., 2016. Geochemistry of basalts from small eruptive centers near Villarrica stratovolcano, Chile: evidence for lithospheric mantle components in continental arc magmas. Geochim. Cosmochim. Acta 185, 358–382.

Hildreth, W., Moorbath, S., 1988. Crustal contributions to arc magmatism in the Andes of

central Chile. Contrib. Mineral. Petrol. 98, 455–489.
Holm, P.M., Søager, N., Dyhr, C.T., Nielsen, M.R., 2014. Enrichments of the mantle sources beneath the Southern Volcanic Zone (Andes) by fluids and melts derived from abraded upper continental crust. Contrib. Mineral. Petrol. 167, 1004.
Horton, B.K., 2018. Mesozoic-Cenozoic tectonic regimes of th central and southern Andes: response to variations in plate coupling. Tectonics 37, 1–28.
Horton, B.K., Fuentes, F., 2016. Sedimentary record of plate coupling and decoupling during growth of the Andes. Geology 44, 647–650.
Iannelli, S., Fennell, L., Litvak, V.D., Fernández Paz, L., Encinas, A., Folguera, A., 2018. Geochemical and tectonic evolution of Late Cretaceous to early Paleocene magmatism along the Southern Central Andes (35–36°S). J. S. Am. Earth Sci. 1–18. http://dx.doi.org/10.1016/j.jsames.2017.12.008. (in press, corrected proof).
Irvine, T.N., Baragar, W.R.A., 1971. A guide to the chemical classification of the common volcanic rocks. Can. J. Earth Sci. 8, 523–548.
Jacobsen, S.B., Wasserburg, G.J., 1980. Sm–Nd isotopic evolution of chondrites. Earth Planet. Sci. Lett. 50, 139–155.
Kay, S.M., Mpodozis, C., 2002. Magmatism as a probe to the Neogene shallowing of the Nazca plate beneath the modern Chilean flat-slab. J. S. Am. Earth Sci. 15, 39–57.
Kay, S.M., Godoy, E., Kurtz, A., 2005. Episodic arc migration, crustal thickening, subduction erosion, and magmatism in the south-central Andes. Geol. Soc. Am. Bull. 117, 67–88.
Kay, S.M., Burns, W.M., Copeland, P., Mancilla, O., 2006. Upper Cretaceous to Holocene magmatism and evidence for transient Miocene shallowing of the Andean subduction zone under the northern Neuquén Basin. In: Kay, S.M., Ramos, V.A. (Eds.), Evolution of an Andean Margin: A Tectonic and Magmatic View From the Andes to the Neuquén Basin (35°–39°S Lat). Geological Society of America, Special Papers, vol. 407. pp. 19–60.
Klohn, C., 1960. Geología de la Cordillera de los Andes de Chile (Provincias de Santiago, Colchagua y Curicó). In: Instituto de Investigaciones Geológicas, Boletín 8, Santiago, (95 pp.).
Kuno, H., 1966. Lateral variation of basaltic magma type across continental margins and island arcs. Bull. Volcanol. 29, 195–222.
Llambías, E.J., Rapela, C.W., 1989. Las volcanitas de Collipilli, Neuquén (37°S) y su relación con otras unidades paleogenas de la cordillera. Rev. Asoc. Geol. Argent. 44, 224–236.
Ludwig, K.R., 2008. Manual for Isoplot 3.7. Berkeley Geochronology Center (Special Publication, 77 pp.).
Maksaev, V., Munizaga, F., Tassinari, C., 2014. Timing of the magmatism of the paleo-Pacific border of Gondwana: U-Pb geochronology of Late Paleozoic to Early Mesozoic igneous rocks of the north Chilean Andes between 20° and 31°S. Andean. Geology 41, 447–506.
Maloney, K.T., Clarke, G.L., Klepeis, K.A., Quevedo, L., 2013. The Late Jurassic to present evolution of the Andean margin: drivers and the geological record. Tectonics 32, 1049–1065.
Mamani, M., Wörner, G., Sempere, T., 2010. Geochemical variations in igneous rocks of the Central Andean orocline (13°S to 18°S): tracing crustal thickening and magma generation through time and space. Geol. Soc. Am. Bull. 122, 162–182.
Marinovic, N., García, M., 1999. Hoja Pampa Unión, Región de Antofagasta. In: Mapas Geológicos, vol. 9 Sernageomin, Santiago.
Marinovic, N., Cortés, J., García, M., 1996. Estudio Geológico Regional de la zona comprendida entre Sierra del Buitre y Pampa San Román. Sernageomin, IR-96-8, Santiago (156 pp.).
Martínez-Pardo, R., Osorio, R., 1963. Consideraciones preliminares sobre la presencia de Carófitas fósiles en la Formación Colimapu. In: Revista Minerales, vol. 82. Departamento de Geología, Universidad de Chile, Santiago, pp. 28–43.
Mateo, M.P., Montero, D., Leal, P., Ramos, V.A., 2011. Petrografía y geoquímica del magmatismo Cretácico Superior-Eoceno en el área de Pichaihue, Provincia de Neuquén. Rev. Asoc. Geol. Argent. 68, 173–184.
Matthews, S., Espinoza, F., Cornejo, P., Venegas, C., 2010. Carta Altamira, Regiones de Antofagasta y Atacama. In: Carta Geológica de Chile, Serie Geología Básica, vol. 121 Sernageomin (66 pp.).
Mescua, J., Giambiagi, L.B., Ramos, V.A., 2013. Late Cretaceous Uplift in the Malargüe fold-and-thrust belt (35°S), southern Central Andes of Argentina and Chile. Andean Geol. 40, 102–116.
Mescua, J., Giambiagi, L.B., Tassara, A., Gimenez, M., Ramos, V.A., 2014. Influence of pre-Andean history over cenozoic foreland deformation: structural styles in the malargüe fold-and-thrust belt at 35°S, Andes of Argentina. Geosphere 10, 585–609.
Miyashiro, A., 1974. Volcanic rock series in island arc and continental margins. Am. J. Sci. 274, 321–355.
Mosolf, J., 2013. Stratigraphy, Structure, and Geochronology of the Abanico Formation in the Principal Cordillera, Central Chile: Evidence of Protracted Volcanism and Implications for Andean Tectonics. Department of Earth Sciences, University of California (Ph.D. Thesis, 152 pp.).
Mosolf, J., Gans, P.B., Wyss, A.R., Cottle, J.M., 2011. Detailed geologic field mapping and radiometric dating of the Abanico Formation in the Principal Cordillera, central Chile: evidence of protracted volcanism and implications for Cenozoic tectonics. In: AGU Fall Meeting, San Francisco, pp. #V13C-2623.
Mpodozis, C., Allmendinger, R.W., 1993. Extensional tectonics, Cretaceous Andes, northern Chile (27°S). Geol. Soc. Am. Bull. 105, 1462–1477.
Mpodozis, C., Ramos, V.A., 1989. The Andes of Chile and Argentina. In: Ericksen, G.E., Cañas, M.T., Reinemund, J.A. (Eds.), Geology of the Andes and its Relation to Hydrocarbon and Mineral Resources. Circum-Pacific Council for Energy and Mineral Resources, Texas, Earth Science Series, vol. 11. pp. 59–90.
Müller, R.D., Seton, M., Zahirovic, S., Williams, S.E., Matthews, S.J., Wright, N.M., Shepard, G.E., Maloney, K.T., Barnett-Moore, N., Bower, D.J., Cannon, J., 2016. Ocean basin evolution and global-scale reorganization events since Pangea breakup. Annu. Rev. Earth Planet. Sci. 44, 107–138.
Nakamura, N., 1974. Determination of REE, Ba, Fe, Mg, Na and K in carbonaceous and ordinary chondrites. Geochim. Cosmochim. Acta 38, 757–775.
Nyström, J.O., Vergara, M., Morata, D., Levi, B., 2003. Tertiary volcanism in central Chile (33°15′–33°45′S): a case of Andean magmatism. Geol. Soc. Am. Bull. 115, 1523–1537.
Ori, G.G., Friend, P.F., 1984. Sedimentary basins formed and carried piggyback on active thrust sheets. Geology 12, 475–478.
Pardo, M., Comte, D., Monfret, T., 2002. Seismotectonic and stress distribution in the central Chile subduction zone. J. S. Am. Earth Sci. 15, 11–12.
Paton, C., Woodhead, J., Hellstrom, J., Hergt, J., Greig, A., Maas, R., 2010. Improved laser ablation U-Pb zircon geochronology through robust downhole fractionation correction. Geochem. Geophys. Geosyst. 11, Q0AA06.
Pearce, J.A., 1983. Role of the sub-continental lithosphere in magma genesis at active continental margins. In: Hawkesworth, C.J., Norry, M.J. (Eds.), Continental Basalts and Mantle Xenoliths. Shiva Publications, Nantwich, Cheshire, pp. 230–249.
Persico, M., 2016. La Unidad Guanaco en el valle del río Tinguiririca (34°55′S): características estratigráficas y geoquímicas e implicancias tectónicas para el Cretácico Tardío en el margen Andino. Departamento de Geología, Universidad de Chile (Geologist Thesis, 75 pp.).
Persico, M., Muñoz, M., Tapia, F., Arellano, P., Farías, M., 2015. Hallazgo de estratos de edad Cretácico Tardío en el curso alto del río Tinguiririca (~34°55'S). Parte I: Principales Características. In: XIV Congreso Geológico Chileno, La Serena, Digital Abstracts.
Petrus, J., Kamber, B., 2012. VizualAge: a novel approach to laser ablation ICP-MS U-Pb geochronology data reduction. Geostand. Geoanal. Res. 36, 247–270.
Piquer, J., Castelli, J., Charrier, R., Yáñez, G., 2010. El Cenozoico del alto río Teno, Cordillera Principal, Chile central: estratigrafía, plutonismo y su relación con estructuras profundas. Andean Geol. 37, 32–53.
Platt, J.P., 1986. Dynamics of orogenic wedges and the uplift of high-pressure metamorphic rocks. Geol. Soc. Am. Bull. 97, 1037–1053.
Ramos, V.A., Folguera, A., 2005. Tectonic evolution of the Andes of Neuquén: constraints derived from the magmatic arc and foreland deformation. In: The Neuquén Basin, Argentina. Geological Society, London, Special Publications, vol. 252. pp. 15–35.
Ramos, V.A., Cegarra, M., Cristallini, E., 1996. Cenozoic tectonics of the high Andes of west-central Argentina (30–36°S latitude). Tectonophysics 259, 185–200.
Schellart, W.P., 2008. Overriding plate shortening and extension above subduction zones: a parametric study to explain formation of the Andes Mountains. Geol. Soc. Am. Bull. 120, 1441–1454.
Segemar, 1997. Mapa Geológico de Argentina, 1:2500000. Servicio Geológico Minero Argentino.
Sernageomin, 2002. Mapa Geológico de Chile, 1:1000000. Servicio Nacional de Geología y Minería.
Seton, M., Müller, R.D., Zahirovic, S., Gaina, C., Torsvik, T., Shepard, G.E., Talsma, A., Gurnis, M., Turner, M., Maus, S., Chandler, M., 2012. Global continental and ocean basin reconstructions since 200 Ma. Earth-Sci. Rev. 113, 212–270.
Sláma, J., Košlera, J., Condon, D., Crowley, J., Gerdes, A., Hanchar, J., Horstwood, M., Morris, G., Nasdala, L., Norberg, N., Schaltegger, U., Schoene, B., Tubrett, M., Whitehouse, M., 2008. Plešovice zircon - a new natural reference material for U–Pb and Hf isotopic microanalysis. Chem. Geol. 249, 1–35.
Söderlund, U., Patchett, P.J., Vervoort, J.D., Isachsen, C.E., 2004. The 176Lu decay constant determined by Lu-Hf and U-Pb isotope systematics of Precambrian mafic intrusions. Earth Planet. Sci. Lett. 219, 311–324.
Solari, L., Gómez-Tuena, A., Bernal, J.P., Pérez-Arvizu, O., Tanner, M., 2010. U-Pb zircon geochronology with an integrated LA-ICP-MS microanalytical workstation: achievements in precision and accuracy. Geostand. Geoanal. Res. 34, 5–18.
Solari, L., González-León, C., Valencia-Moreno, M., Rascón-Heimpel, M., 2017. The Proterozoic of NW Mexico revisited: U–Pb geochronology and Hf isotopes of Sonoran rocks and their tectonic implications. Int. J. Earth Sci. 1–17.
Somoza, R., Ghidella, M., 2005. Convergencia en el margen occidental de América del Sur durante el Cenozoico: subducción de las placas de Nazca, Farallón y Aluk. Rev. Asoc. Geol. Argent. 60, 797–809.
Spagnuolo, M., Folguera, A., Litvak, V.D., Vera, E., Ramos, V.A., 2012. Late Cretaceous arc rocks in the Andean retroarc region at 36.5°S: evidence supporting a Late Cretaceous slab shallowing. J. S. Am. Earth Sci. 38, 44–56.
Steinman, G., 1929. Geologie von Peru. Karl Winters Universitäts-Buchhandlung, Heidelberg (448 pp.).
Stern, C.R., 2004. Active Andean volcanism: its geologic and tectonic setting. Rev. Geol. Chile 31, 161–206.
Stern, C.R., Amini, H., Charrier, R., Godoy, E., Hervé, F., Varela, J., 1984. Petrochemistry and age of rhyolitic pyroclastic flows which occur along the drainage valleys of the río Maipo and río Cachapoal (Chile) and the río Yaucha and río Papagayos. Andean Geol. 23, 39–52.
Talling, P.J., Lawton, T.F., Burbank, D.W., Hobbs, R.S., 1995. Evolution of a latest Cretaceous-Eocene nonmarine deposition in the Axhandle piggyback basin of central Utah. Geol. Soc. Am. Bull. 107, 297–315.
Tanaka, T., Togashi, S., Kamioka, H., Amakawa, H., Kagami, H., Hamamoto, T., Yuhara, M., Orihashi, Y., Yoneda, S., Shimizu, H., Kunimaru, T., Takahashi, K., Yanagi, T., Nakano, T., Fujimaki, H., Shinjo, R., Asahara, Y., Tanimizu, M., Dragusanu, C., 2000. JNdi-1: a neodymium isotopic reference in consistency with LaJolla neodymium. Chem. Geol. 168, 279–281.
Tapia, F., 2015. Evolución tectónica y configuración actual de los Andes Centrales del Sur (34°45′-35°30′S). Departamento de Geología, Universidad de Chile (Ph.D. Thesis, 165 pp.).
Tapia, F., Muñoz, M., Farías, M., Arellano, P., Persico, M., 2015. Hallazgo de estratos de edad Cretácico Tardío en el curso alto del río Tinguiririca (~34°55′S). Parte II:

implicancias tectónicas. In: XIV Congreso Geológico Chileno, La Serena, Digital Abstracts.
Tassara, A., Echaurren, A., 2012. Anatomy of the Andean subduction zone; three-dimensional density model upgraded and compared against global-scale models. Geophys. J. Int. 189, 161–168.
Tunik, M., Folguera, A., Naipauer, M., Pimentel, M., Ramos, V., 2010. Early uplift and orogenic deformation in the Neuquén Basin: constraints on the Andean uplift from U–Pb and Hf isotopic data of detrital zircons. Tectonophysics 489, 258–273.
Vergani, G.D., Tankard, A.J., Belotti, H.J., Welsink, H.J., 1995. Tectonic evolution and paleogeography of the Neuquén Basin, Argentina. In: Tankard, A.J., Suárez, R., Welsink, H.J. (Eds.), Petroleum Basins of South America. American Association of Petroleum Geologists, Memoir, vol. 62. pp. 383–402.
Vermeesch, P., 2012. On the visualization of detrital age distributions. Chem. Geol. 312–313, 190–194.
Vervoort, J.D., Blichert-Toft, J., 1999. Evolution of the depleted mantle: Hf isotope evidence from juvenile rocks through time. Geochim. Cosmochim. Acta 63, 533–556.
Wiedenbeck, M., Alle, P., Corfu, F., Griffin, W.L., Meier, M., Oberli, F., von Quadt, A., Roddick, J.C., Spiegel, W., 1995. 3 natural zircon standards for U-Th-Pb, Lu-Hf, trace-element and REE analyses. Geostand. Geoanal. Res. 19, 1–23.
Wilson, M., 1989. Igneous Petrogenesis, A Global Tectonic Approach. Springer Netherlands (466 pp.).
Zamora Valcarce, G., Zapata, T., del Pino, D., Ansa, D., 2006. Structural evolution and magmatic characteristics of the Agrio fold-and-thrust belt. In: Kay, S.M., Ramos, V.A. (Eds.), Evolution of an Andean Margin: A Tectonic and Magmatic View From the Andes to the Neuquén Basin (35°–39°S Lat). Geological Society of America, Special Papers, vol. 407. pp. 125–145.
Zapatta, F., 1995. Nuevos antecedentes estratigráficos y estructura del área de Termas del Flaco, Valle del Río Tinguiririca, VI Región, Chile. Departamento de Geología, Universidad de Chile (Geologist Thesis, 122 pp.).